THE FLORIDA STATE UNIVERSITY

COLLEGE OF ARTS AND SCIENCES

THE CONNECTIVITY OF EDDY VARIABILITY

IN THE CARIBBEAN SEA,

THE GULF OF MEXICO,

AND THE ATLANTIC OCEAN

By

SYLVIA J. MURPHY

A Thesis submitted to the
Department of Oceanography
in partial fulfillment of the
requirements for the degree of
Master of Science

Degree Awarded:
Spring Semester, 1996

invoking an instability mechanism. Thus the eddy shedding frequency was not determined by a flow instability, but by the time required for the Loop to penetrate into the Gulf of Mexico and bend westward into an unstable configuration. This time scale involved in the development of the unstable configuration was closely linked to the time required for the train of anticyclonic and cyclonic eddies that appear in the deviation form the long term mean circulation, to propagate one wavelength at the non-dispersive internal Rossby wave speed.

The connection between Loop Current eddy shedding and Caribbean eddies itn the numerical simulations is evident graphically in Figures 11a, b, 21 and 22 In figure 21 there are 16 observable Loop Current Eddies. Of those 16, 56% (9) can be observed to be directly linked to Caribbean eddies. For simualtion 2 (Figure 22) 30% (7) of the 23 Loop Current Eddies are linked. The connectivity of the Caribbean eddies to the Loop Current Eddy is also quantifiable by a cross correlation between the layer thickness time series of increment 27 (representing the loop current eddy) and the first increment (representing the initial input of eddies into the Caribbean) results in a significant correlation value of .45 at a lag of 11.4 months for simulation 1.

Although the Loop Current Eddy continues to form and detach even during periods of weak or no Caribbean eddies, Figure 23 indicates that during the low period of the intradecadal cycle, the Loop Current Eddies are also weakened. This is most likely due to a weakening of the flow through the Yucatan Channel.

There is a paucity of Caribbean observational data in the Caribbean with which to conduct a model-data comparison. In one case, eddies observed in the reduced gravity simulation can be related to eddies observed by Geosat. with which to conduct a model-data comparison. In one case, eddies observed in the reduced gravity simulation can be related to eddies observed by Geosat.

It should be noted that the model eddies are not caused by a deterministic response to the atmospheric forcing, and therefore a comparison between observational and model eddies can be done only in a statistical sense, not as individual eddies.

Nystuen and Andrade [1993] reported two eddies tracks (Figure 24 and 25) over three days in the month of July, 1987 and April, 1988. The Geosat eddy A in 1987 tracks approximately one degree further south and two degrees further west than the model eddy. Intensity differences vary from between 0.15 and 0.25 m. The average propagating velocities of the Geosat eddies is 0.15 m/s which matches the average model propagation velocity. This supports the idea put forth by Nystuen and Andrade, [1993] that the eddies are interacting with mean current since the average velocity is significantly slower than the Lagrangian drifters (@ 0.50 m/s) deployed by Molinari et al. [1981] and Kinder [1983].

For the second Geosat sequence, the satellite eddies track one degree further north, and two degrees further east than the model eddies. Intensity variations are approximately the same as the previous sequence.

Finally, several cross-correlations were done between the Caribbean and Gulf of Mexico and transport of the Florida Current at 27 degrees N (STACS). These results are reported due to the continued interest in understanding the transport varibility at STACS.

A cross correlation between transport through the Yucatan Channel and transport at STACS yielded a value of 0.64 at a lag of 15 days for simulation 1 and 0.77 at lag 15 days for simulation 2. No significant correlation was found between the Loop Current eddy shedding and transport at STACS.

correlation was found between the Loop Current eddy shedding and transport at STACS.
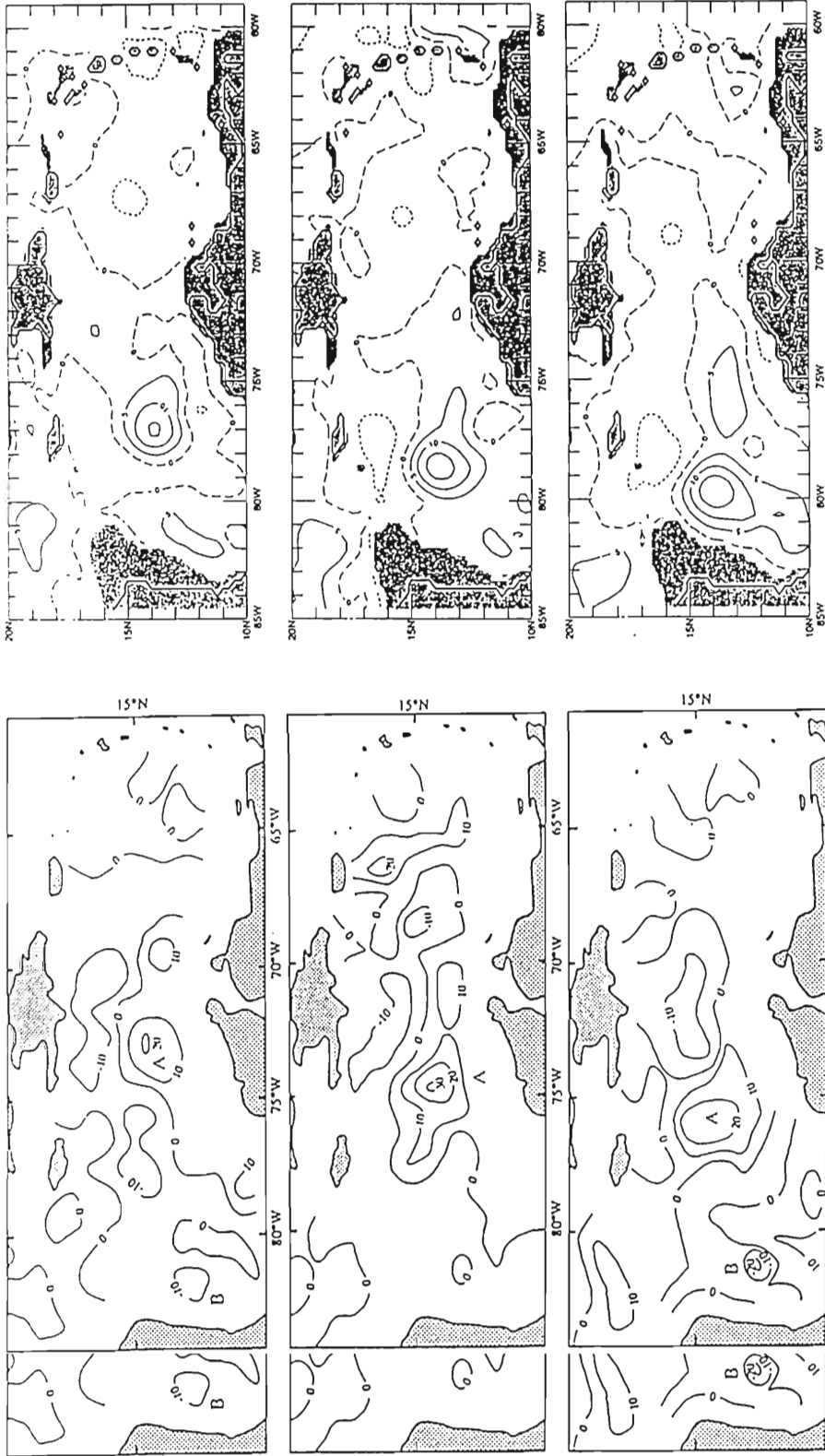
Fig. 24. (a) Geosat SSH anomalies for June 17 to July 21, 1987 from Nystuen and Andrade [1993]. (b) Corresponding SSH anomalies from the reduced gravity simulation.
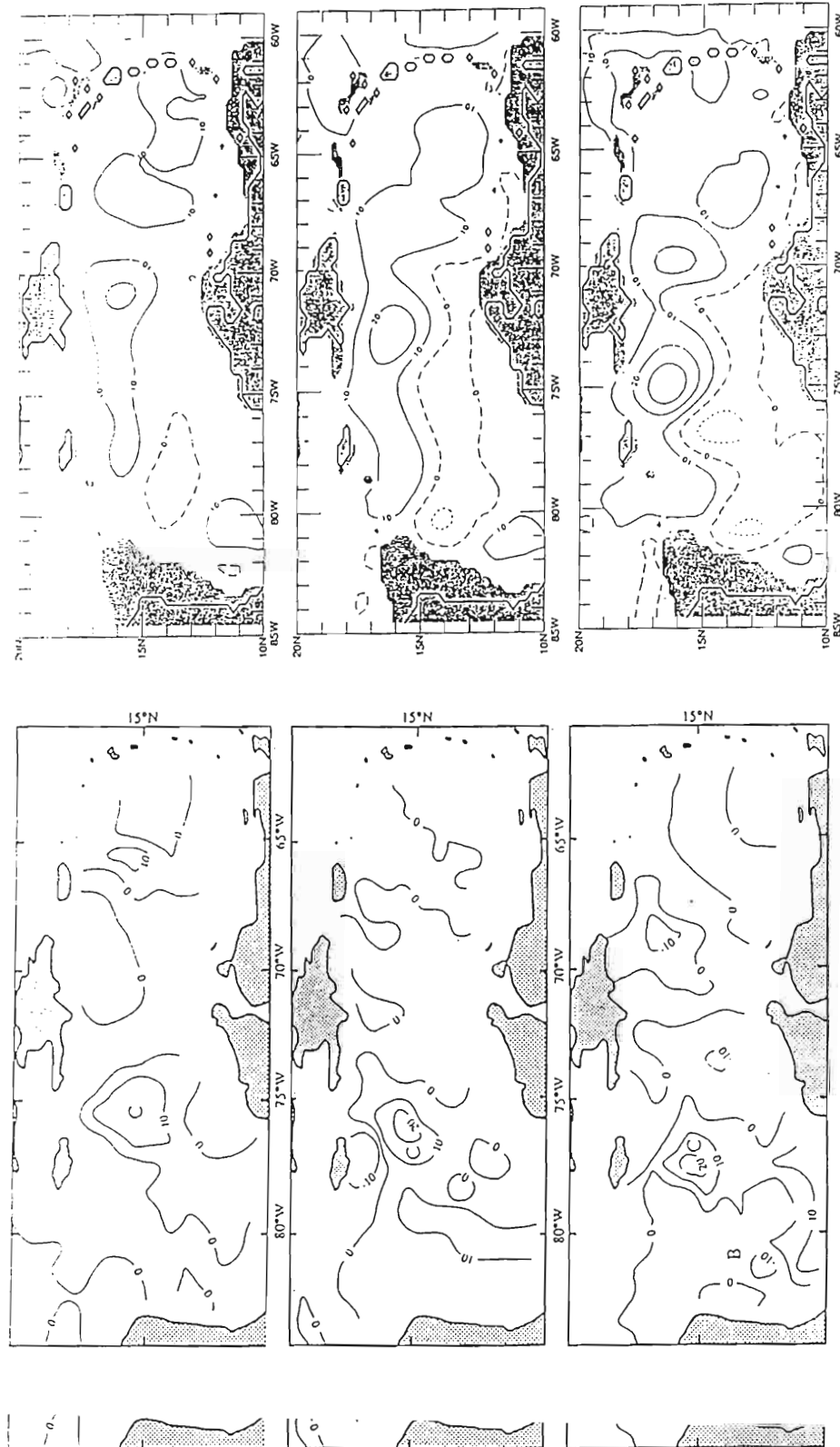
Fig. 25. (a) Geosat anomalies for April 13 to May 17, 1988. (b) Corresponding SSH anomalies from the reduced gravity simulation.

4

SUMMARY AND CONCLUSIONS

The connectivity of mesoscale variability in the Atlantic Ocean, Caribbean, and Gulf of Mexico has been studied using three simulations by the Naval Research Laboratories global ocean model. Two simulations possess a horizontal resolution of 1/4° and are forced by ECMWF hybrid winds. They are 5.5-layer reduced gravity and 6-layer finite depth with realistic bottom topography. The third simulation is a 1/2° linear model. Although no eddies are observed in the linear simulation, it is useful for determining the influence of the wind forcing on the current structure. Mesoscale features are observed in the first two model simulations. These features dominate the surface oceanography of the Caribbean (Figures 6-11) and influence the variability of the Loop Current Eddies in the Gulf of Mexico. At present, no other study has revealed such an extensive eddy field for the Caribbean.

Caribbean eddies are generated on the western side of the Lesser Antilles arc. Their relationship to the Atlantic Ocean is best observed in Figure 6a. Brazil retroflection eddies periodically impact the Lesser Antilles and decay. The numerical simulations show some of their potential vorticity being advected through the island passages.

The Guyana current which feeds into the Caribbean (Figure 2) possesses an intradecadal cycle which is concurrently observed in both the
The Guyana current which feeds into the Caribbean (Figure 2) possesses an intradecadal cycle which is concurrently observed in both the

44

transports of the Caribbean passages and the Caribbean current. During the peak in the transport through the St. Vincent passage, a shear maxima occurs (Figure 17), which allows the eddies form. The potential vorticity advected through the passage acts as a finite amplitude perturbation for horizontal shear instability. The initial intensity of the Caribbean eddies is weak compared to their Brazil Retroflection counterparts, but as the Caribbean eddies transit the basin, they intensify into large scale features (average diameter equals 330 km for the reduced gravity simulation, see Results for details). This intensification is due to the increased shear within the Caribbean current along the axis of eddy propagation (Figure 18)

Beta Rossby number calculations for both simulations also indicate that the eddies form as the result of barotropic versus baroclinic instability. The average beta Rossby number for the reduced gravity simulation was 0.466 while the average for the finite depth simulation was 0.771. A beta Rossby number of order one is indicative of barotropic instability while a beta Rossby number of order ten is indicative of baroclinic instability.

In their transits across the Caribbean, the mesoscale features can be tracked along a fairly narrow corridor (Figure 12) which represents an ensemble of eddy tracks. Along this corridor, the eddies possess an annual and an intradecadal cycle. The latter is related to the strength of the currents and the wind stress curl as mentioned above. The average kinetic energy for the Caribbean basin also possesses the intradecadal cycle (Figure 14a)

On average, the eddies propagate at 0.15 m/s and take ten months to transit the basin from their generation site near the Lesser Antilles to the Yucatan Channel. The eddies then pass through the channel, often forming a continuous feature with the Loop Current Eddy (Figures 6a, b). In the reduced Yucatan Channel. The eddies then pass through the channel, often forming a continuous feature with the Loop Current Eddy (Figures 6a, b). In the reduced

gravity simulation, 56% of the Loop Current Eddies could be directly linked to Caribbean eddies. 20% of the variance (r squared) in Loop Current Eddies is related to the eddies at their formation site near the Lesser Antilles. This is a new factor in Loop Current dynamics that must be considered in subsequent studies or models of the Gulf of Mexico.

Cyclonic eddies are observed to enter the Caribbean along an axis of 12° N and transit westward until they impact Central America where they are deflected southward, merge, and intensify. This process is particularly significant for Latin American pollution or fisheries models which have traditionally been forced by coastal winds, or by an off shore model which in turn was forced by regional winds. Many of the coastal processes that effect the countries that border the southern Caribbean will be strongly affected by the cyclonic features that originate outside of the region. These must be considered in any effort to model the Caribbean littoral zone.

Other than limited drifter tracks, there is a scarcity of observational data in the Caribbean region. The reduced gravity model matches well with the eddies reported by Nystuen and Andrade [1993] (Figures 24 and 25).

Both the reduced gravity and finite depth simulations show the same complex eddy fields. These simulations were forced by daily winds, which contained the variability necessary to generate the currents and equatorial eddies that transit up the Brazil coast and impact the Lesser Antilles. A model that is forced by a set inflow through the Lesser Antilles [Heburn et al., 1982] will produce some eddies but will not capture the periodicity, connectivity, or cycles of Caribbean eddies. Any successful modeling of the Caribbean must therefore consider the importance of the equatorial Atlantic.

therefore consider the importance of the equatorial Atlantic.

Mesoscale features can increase the uncertainty about the dispersal of fish larvae or pollutants, both of which are important to the developing nations bordering the region. The confinement of the large scale eddies to a narrow track and knowledge of their velocity and destination significantly reduces this uncertainty.

REFERENCES

Cochran, J. D., The Yucatan Current and equatorial currents of the western Atlantic, Unpublished report, Dept. of Oceanography, Texas A&M Univerisity, Ref. (65-17T), 20-27, 1965.

Didden, N. and F. Schott, Eddies of the North Brazil Current retrflection region observed by Geosat altimetry, J. Geophys. Res., 98(C11), 20,121-20,131, 1993.

Duncan, C. P., S. G. Schladow, and W. G. Williams, Surface currents near the Greater and Lesser Antilles, Intl. Hydro. Rev., LIX (2), 67-78, 1982.

Fratantoni, D. M., W. E. Johns, and T. L. Townsend, Rings of the North Brazil Current: their structure and behavior inferred from observations and a numerical simulation, J. Geophys. Res., 100(C6), 10,6333-10,654, 1995

Fu, L. L., and B. Holt, Some examples of detection of oceanic mesoscale eddies by the SEASAT synthetic-aperature radar, J. Geophys. Res., 88(C3), 1844-1852, 1983.

Heburn, G. W., T. H. Kinder, J. H. Allender, and H. E. Hurlburt, A numerical model of eddy generation in the southeastern Caribbean Sea, in Hydrodynamics of Semi-Enclosed Seas,, edited by J.C.L. Nihoul, pp. 299-328, Elsevier, Amsterdam, 1982.

Hurlburt, H. E., and J. D. Thompson, A numerical study of Loop Current intrusions and eddy shedding, J. Phys. Oceanogr., 10, 1611-1651, 1980.

Hurlburt, H. E., and J. D. Thompson, The dynamics of the Loop Current and shed eddies in a numerical model of the Gulf of Mexico. In: Hydrodynamics of Semi-Enclosed Seas, J. C. J. Nihoul, ed., Elsevier Scientific Publishing Company, Amsterdam, 243-297, 1982.

Hurlburt, H. E., J. D. Thompson, Preliminary results from a numerical study of the New England Seamount Chain influence on the Gulf Stream. In: Predictability of Fluid Motions. G. Holloway and B. J. West, eds., American Institute of Physics, New York, 489-504, 1984.
study of the New England Seamount Chain influence on the Gulf Stream. In: Predictability of Fluid Motions. G. Holloway and B. J. West, eds., American Institute of Physics, New York, 489-504, 1984.

Ingham, M. C., and C. V. W. Mahnken, Turbulence and Productivity near St. Vincent Island, BWI. A premilinary report. <u>Carib.J. Sci.</u>, 6(3-4): 83-87, 1966

Johns, W. E., T. N. Lee, F. A. Schott, R. J. Zantopp, and R. H. Evans, The North Brazil Current retroflection: Seasonal structure and eddy variability, <u>J. Geophys. Res</u>., 95(C12), 22,103-22,120, 1990.

Kinder, T. H., Shallow currents in the Caribbean Sea and Gulf of Mexico as observed with stellite-tracked drifters. <u>Bull. Mar. Sci.</u>, 33(2): 239-246, 1983.

Kinder, T. H., G. W. Heburn, and A. W. Green, Some aspects of the Caribbean circulation, <u>Marine Geology</u>, 68, 25-52, 1985.

Lemming, T. D., Eddies west of the Southern Lesser Antilles, In: <u>Symposium on Investigations and Resources of the Caribbean Sea and Adjacent Regions</u>. UNESCO, Paris, pp. 113-120, 1971.

Leipper, D. F., A sequence of current pattern in the Gulf of Mexico, <u>J. Geophys. Res</u>., 18. 937-948, 1970.

Levitus, S., <u>Climatological atlas of the world ocean</u>, NOAA Professional Paper 13 , NOAA, US Department of Commerce, 173 pp, 1982.

Maul, G. A. (Ed), <u>Climate change in the Intra-Americas Sea</u>, 389 pp., Routledge, Chapman and Hall, New York, 1993.

Maul, G. A., and F. M. Vukovich, The relationship between variations in the Gulf of Mexico Loop Current and the Straits of Florida volume transport, <u>J. Phys. Oceanogr.</u>, 23, 785-796, 1993.

McWilliams, J. C. and G. R. Flierl, On the evolution of isolated, nonlinear vortices. <u>J. Phys. Oceanogr.</u>, 9, 1155-1182, 1979.

Mesinger, F., and A. Arakawa, <u>Numerical methods used in atmospheric models</u>, GARP Publ. Ser. 17, World Meteorological Organization, 64 pp, 1976.

Metzger, et al., Hindcasting of wind-driven anomalies using a reduced-gravity global ocean model, <u>Mar. Technol. Soc. J.</u>, 26 (2), 23-32, 1992.

Metzger, et al., <u>Hindcasting wind-driven anomalies using reduced-gravity global ocean models with 1/2° and 1/4° resolution</u>, Stennis Space Center, MS, Naval Research Laboratory report 7323--93-9444,
Metzger, et al., <u>Hindcasting wind-driven anomalies using reduced-gravity global ocean models with 1/2° and 1/4° resolution</u>, Stennis Space Center, MS, Naval Research Laboratory report 7323--93-9444, 1994.

Molinari, R. L., M. Spillane, I. Brooks, D. Atwood, and C. Duckett, Surface currents in the Caribbean Sea as deduced from Lagrangian observations, J. Geophys. Res., 86(C7), 6537-6542, 1981.

NOAA, ETOPO5 digital relief of the surface of the earth, Data Announcement 86-MGG-07, National Geophysical Data Center, Washington, D. C., 1986.

Nystuen, J. A., and C. A. Andrade, Tracking mesoscale ocean features n the Caribbean Sea using Geosat altimetry, J. Geophys. Res., 98(C5), 8389-8394, 1993.

Richardson, P. L., G. E. Hufford, R. Limebuger, and W. S. Brown, North Brazil Current retroflection eddies, J. Geophys. Res., 99(C3), 5081-5093, 1994.

Shriver, J. F., and H. E. Hurlburt, The contribution of the global thermohaline circulation to the Pacific to Indian Ocean throughflow via Indonesia, submitted to J. Geophys. Res., May 1995.

Sturges, W., The spectrum of Loop Current variability from gappy data, J. Phys. Oceanogr., 22, 1245-1256, 1992.

Vukovich, F.M., B. W. Crissman, M. Bushnell, W. J. King, Some aspects of the oceanography of the Gulf of Mexico using satellite and in situ data, J. Geophys. Res., 84(C12), 7749-7768, 1979.

Vukovich, F.M, Loop Current boundary variations, J. Geophys. Res., 93(C12), 15,585-15,591, 1988.

Vukovich, F. M., An updated evaluation of the Loop Current's eddy-shedding frequency, J. Geophys. Res., 100(C5), 8655-8659, 1995.

Wallcraft, A. J., The Navy Layered Ocean Model User's Guide, Stennis Space Center, MS, NOARL Report 25, 21pp., 1991.

Youtsey, W. J., Report detailing modifications to the 1/8 degree global bathymetry, Sverfrup Technology, Inc., Stennis Space Center, MS, 1993.

BIOGRAPHICAL SKETCH

Sylvia Murphy was born in Watsonville, California on 31 July, 1965. She graduated from Paso Robles High School in June 1983 and graduated with a degree in Marine Science from Jacksonville University in Jacksonville Florida in May 1987. On the same day, she was commissioned as an Ensign in the United States Navy and reported to Surface Warfare Officers School in Coronado, California. Sylvia completed two tours in the Navy. During her three years on board the U.S.S. Acadia (AD-42), she served as First and Second Division Officer, Combat Systems Officer, and Navigator. She also earned her Surface Warfare Qualification. Sylvia then spent three years as Officer in Charge of the Naval Oceanography Command Detachment, Agana, Guam. This detachment provided aviation and general meteorology support to the island of Guam, the Commonwealth of the Northern Mariana Islands, the Federated States of Micronesia, and the Republic of Palau. During this tour, Sylvia had the privilege of observing the eye passage of seven Typhoons. In April 1993 Sylvia returned to civilian life and Florida State University where she completed a Master of Science in Physical Oceanography in October 1995. She is presently employed by Planning Systems Inc. as an assistant staff scientist working with the Naval Research Laboratories coastal modeling effort. She was recently selected for advancement to Lieutenant Commander in the United States Naval Reserve.

in the United States Naval Reserve.
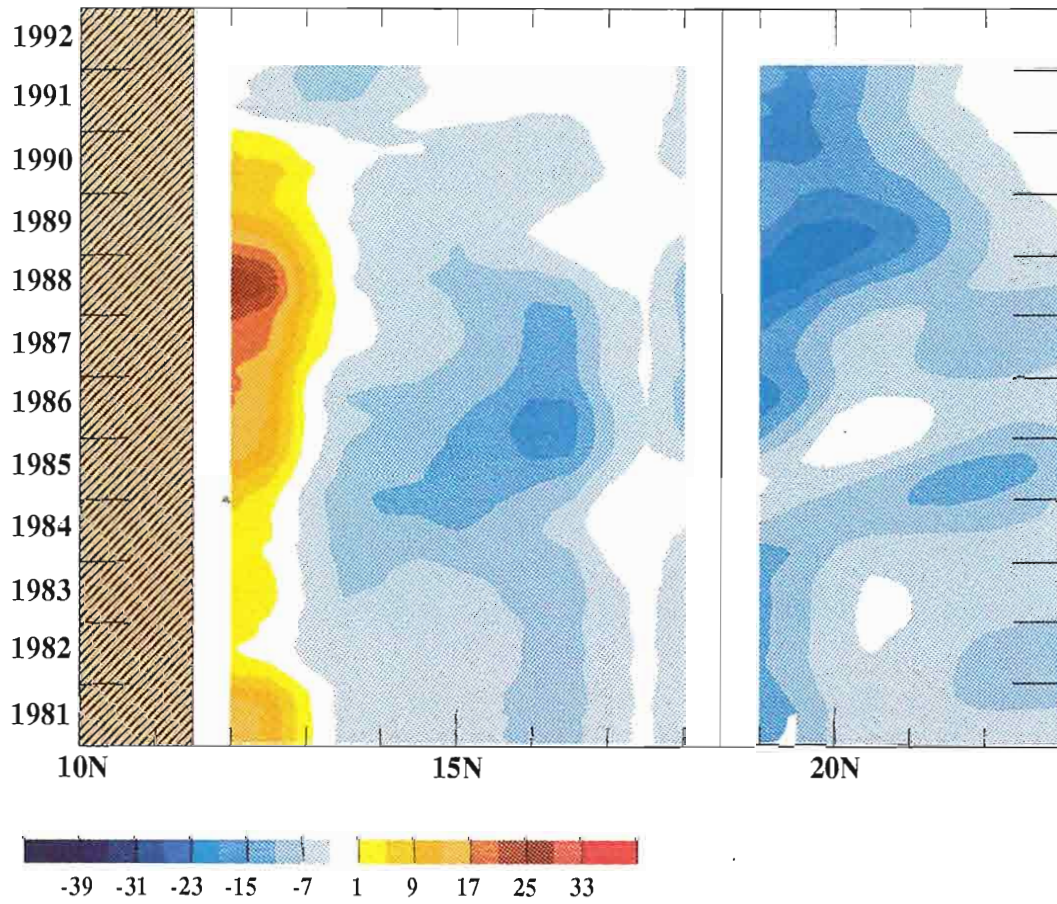
Figure 17. Phase plot of u-component of velocity from linear simulation along an axis of 63.8°W. Latitudinal coverage and smoothing are the same as Figure 15.
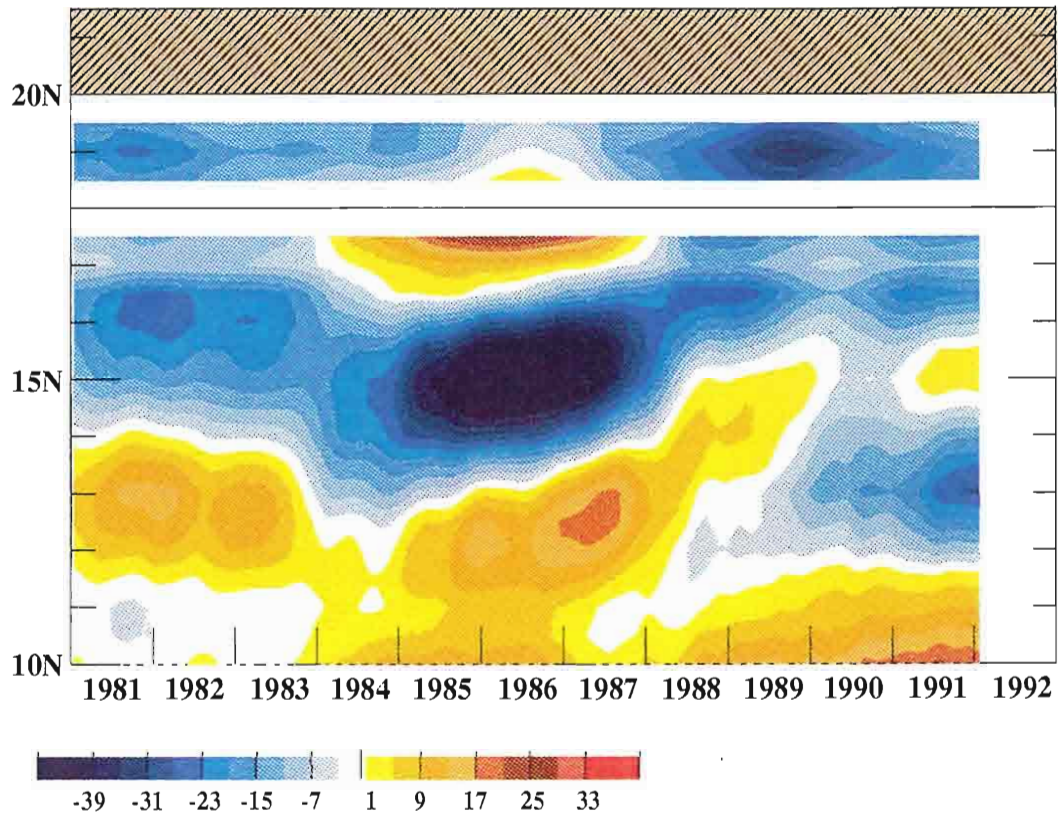
Figure 18. Phase plot of u-component of velocity from linear simulation along an axis of 77.9°W. Latitudinal coverage and smoothing is the same as Figures 15 and 17.
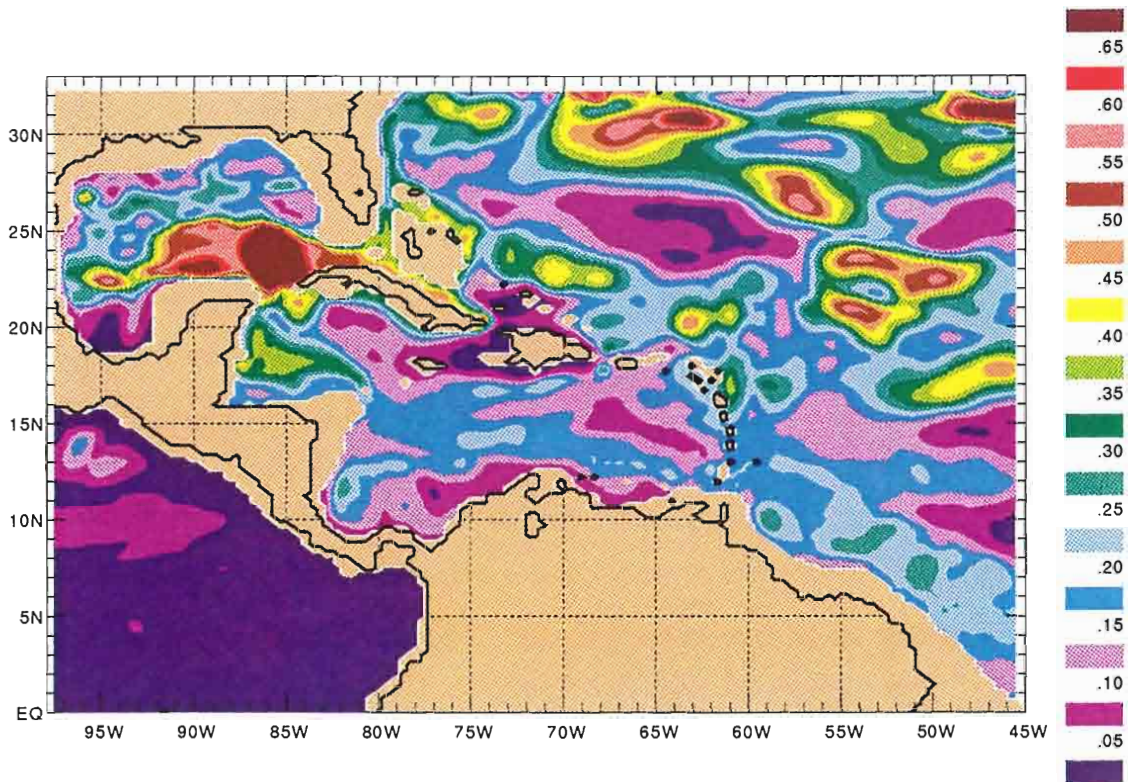
Figure 19. Percent of SSH variability associated with flow instability effects. The field has been normalized by the total SSH variability. Blue and purple areas indicated where wind forcing dominates; orange and red areas indicate regions where flow instability mechanisms are important; contour interval is 5%.

deterministic in nature. Metzger et al., [1994] presents an overview of this technique and the equations involved.

Figure 20 contains time series of windcurl at various latitudes in the Caribbean. Note that several latitudes possess an intradecadal cycle. Of interest is the windstress curl at 12° N. The smoothed time series at this latitude reveals an increase in curl from 1983 to 1987, a corresponding decrease from 1988 to 1990, and a slight increase from 1991 to 1992.

Another indication that the eddies form from barotropic instability vice baroclinic instability is seen in the beta Rossby numbers for both simulations. The beta Rossby number is defined as $\dfrac{v}{\beta r}$ where v is the maximum swirl velocity of an eddy averaged over the entire eddy. β is the variation of the Coriolos force with latitude and r is the mean readius of the eddy as measured by the maximum swirl velocity. The diameter (based on the speed anomaly maximum) and velocities were determined for six representative eddies. The average diameter for simulation 1 was 330 km and for simulation 2 was 365 km. The beta Rossby numbers for these eddies were order one for both simulations with the average for simulation 1 being 0.47 and for simulation 2 being 0.77. A beta Rossby number of order one is indicative of barotropic instability while a beta Rossby number of order ten is indicative of baroclinic instability (see Hurlburt and Thompson 1982, 1984 and McWilliams and Flierl, 1979).

The phase relationship between the kinetic energy in layer 1 and layer 6 of simulation 2 was analyzed. Baroclinic instability has a striking phase relationship. Peaks in layer 6 will lag those in layer 1 if baroclinic instability is involved. No lag in peaks was observed for simulation 2, again eliminating baroclinic instability

involved. No lag in peaks was observed for simulation 2, again eliminating baroclinic instability.
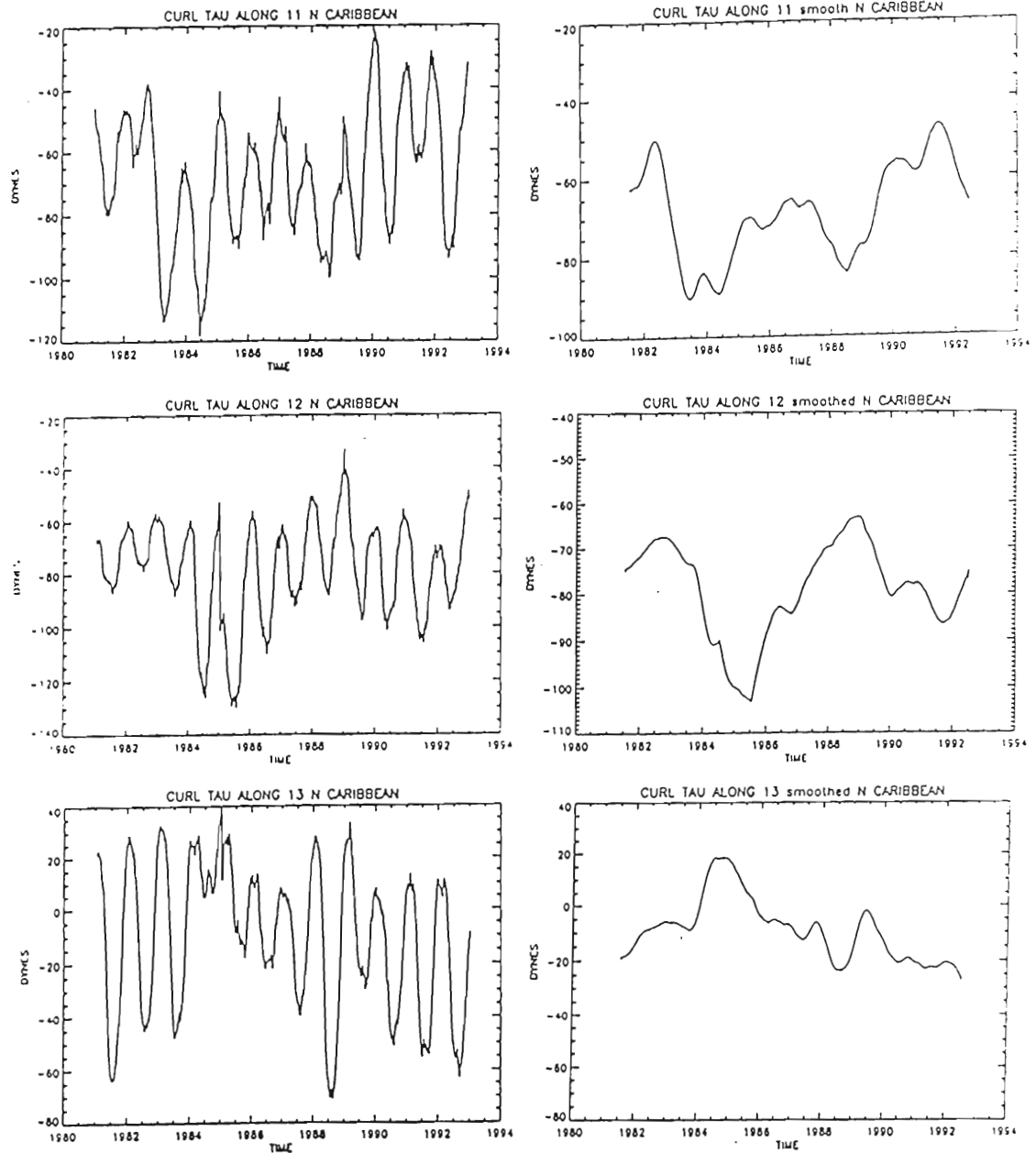
Fig. 20. ECMWF wind stress curl zonally averaged from 64-81° W. Each latitude was also smoothed by a one year running mean.

A Hopfmüller diagram of the eddies in simulation 1 (Figure 21) dramatically displays the intradecadal cycle as well as several other interesting features. The propagation velocity of the eddies along the track is fairly uniform for the first 2000 km of the track (0.13 m/s for simulation 2). At 2000 km (approximately 80° W) the track turns northward and the eddies intensify and accelerate. The average propagation velocity to the Yucatan Channel (3000 km) is 0.15 m/s. The average transit time from the Lesser Antilles to the Yucatan Channel is ten months with values as short as seven months, and as long as seventeen months. The corresponding plot for simulation 2 (Figure 22) is similar with the exception of the Loop Current Eddy shedding frequency.

The frequency for separation of the Loop Current eddies has been pinned down on an order of a year. The data sets of ring separations are gappy and short which hinders statistical analysis and different analyses show variation in spectral peaks. For example, Vukovich, [1995] compiled two data sets, one 22-year data set (1972-1993) and one 17-year data set (1977-1993), from various sources. Sturges [1992] also reported a technique to develop a continuous data set. This method yields a primary spectral peak at 8.5 months, and a secondary peaks at 6, 13.4, and 25 months. Similar bimodal frequencies were reported by Vukovich [1988] and Maul and Vukovich [1993] (6, 10.9, and 17 months); Vukovich [1995] (9, 14 months). Single mode frequencies of 8-9 months were reported by Maul et al. [1985].

It is unclear whether this variability in frequency reflects the natural variability of ring separation or problems associated with the data sets, such as their length. For example, Vukovich [1995] reported a primary mode of 9 months, and a secondary mode of 14 months. The mean

as their length. For example, Vukovich [1995] reported a primary mode of 9 months, and a secondary mode of 14 months. The mean

Reduced Gravity Experiment
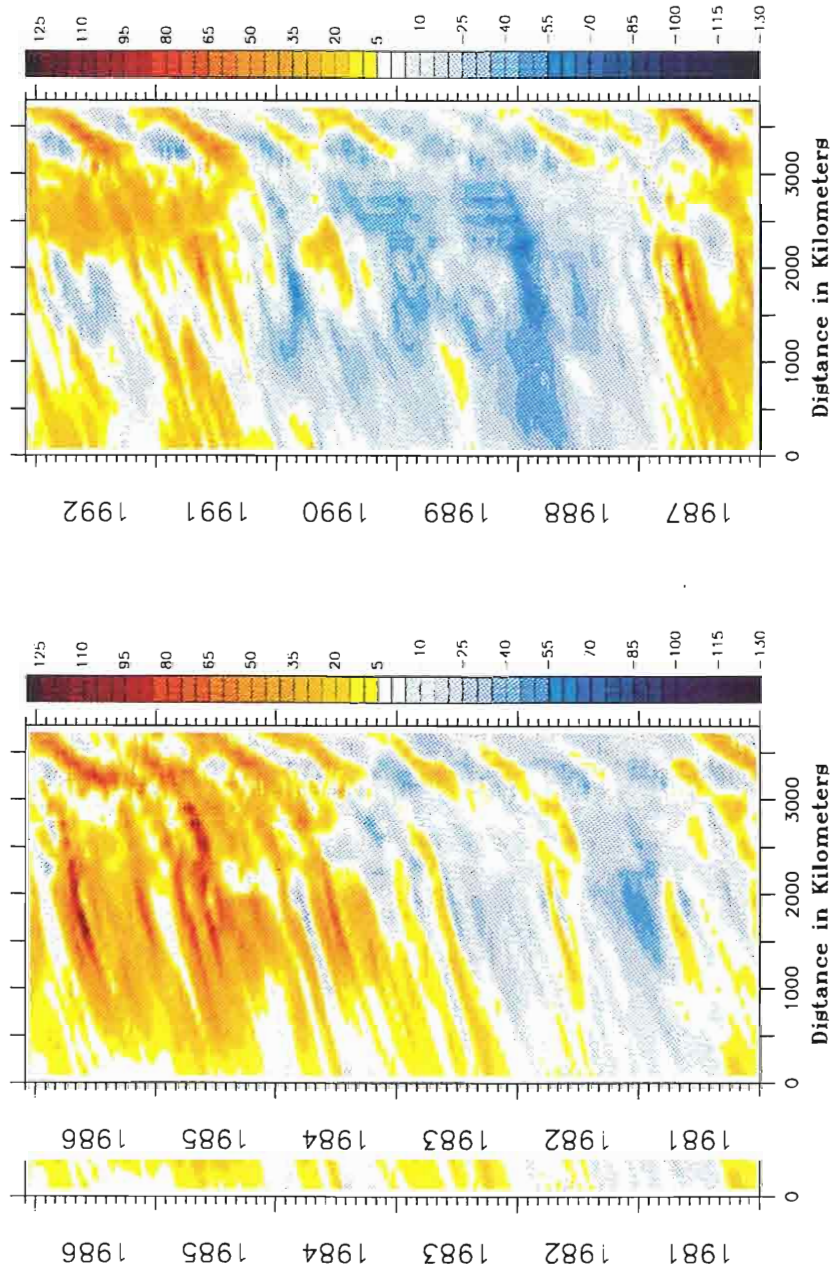
Fig. 2Fig. 21. Hopfmuller plot of upper layer thickness anomaly along corridcorridor in Figure 12. The intradecadal variability is apparent with ewith eddy activity in 1985-86, and little in 1988-89.
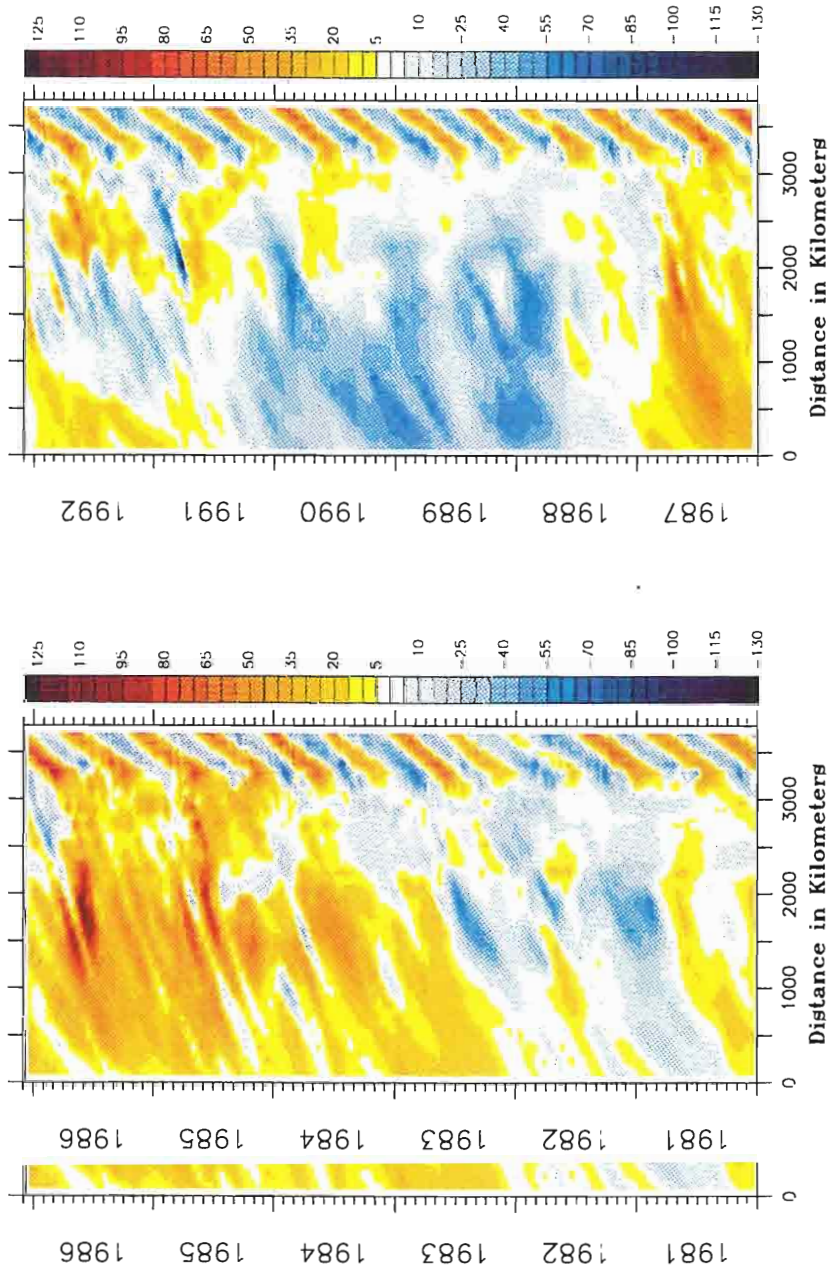
36

Finite Depth Experiment

Fig. 22. Same as Figure 21 but for finite depth simulation.

37

period of the Loop Current Eddy Shedding (11 months) would have a frequency equal to the secondary spectral peak with only one more data occurrence at eleven months, and it would have a frequency equal to the primary spectral peak with only two more data occurrences.

In the 12.5 years of reduced gravity model results, there were eighteen Loop Current Eddies. This number was determined by averaging the reduced gravity upper layer anomalies at 89.8° W from 21.0 to 30.0° N (Figure 23). This resulted in a frequency of 8.3 months between eddies. In the finite depth simulation, there were 24 eddies in twelve years (Figure 22) or, 6.0 months between eddies. The observed eddy shedding frequencies are much more variable than those exhibited in the model [Vukovich, 1995], although 8.3 months matches the primary spectral peaks reported by Maul et al., [1985]; Sturges, [1992]; and Vukovich, [1995].

Historically, ring separation was thought to result from seasonal variations in transport through the Yucatan Channel which affected the penetration distance of the Loop Current into the Gulf of Mexico (Cochran, 1965). Using a set of numerical simulations, Hurlburt and Thompson, [1980, 1982] demonstrated that an eddy shedding period similar to that observed was possible with constant inflow transport. They also demonstrated that a 1.5 layer reduced gravity model was the simplest model that could reproduce the basic eddy-shedding cycle, eliminating baroclinic instability as a determining factor in the periodicity. Instead, they found a horizontal shear instability in the first internal mode. It should be noted that while horizontal shear instability was used to explain the final eddy pinch off in that model, they showed that the westward bending of the Loop Current and its tendency to bend   back   on   itself   could   be   understood   without
showed that the westward bending of the Loop Current and its tendency to
bend   back   on   itself   could   be   understood   without
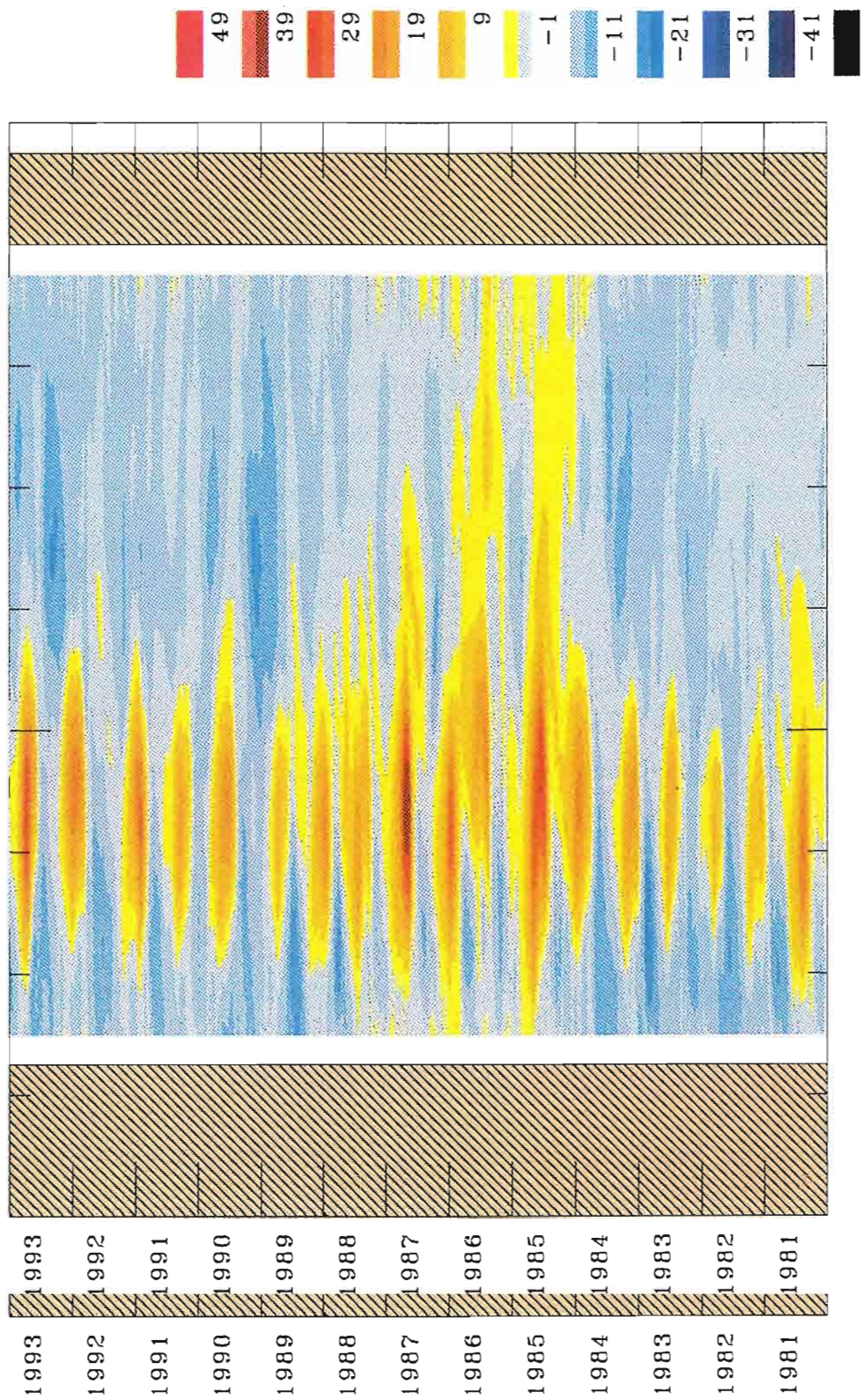
Figure 23. Phase plot of upper layer thickness anomalies from the reduced gravity simulation for 21-31 degrees north. Y-axis is time and X-axis is latitude.
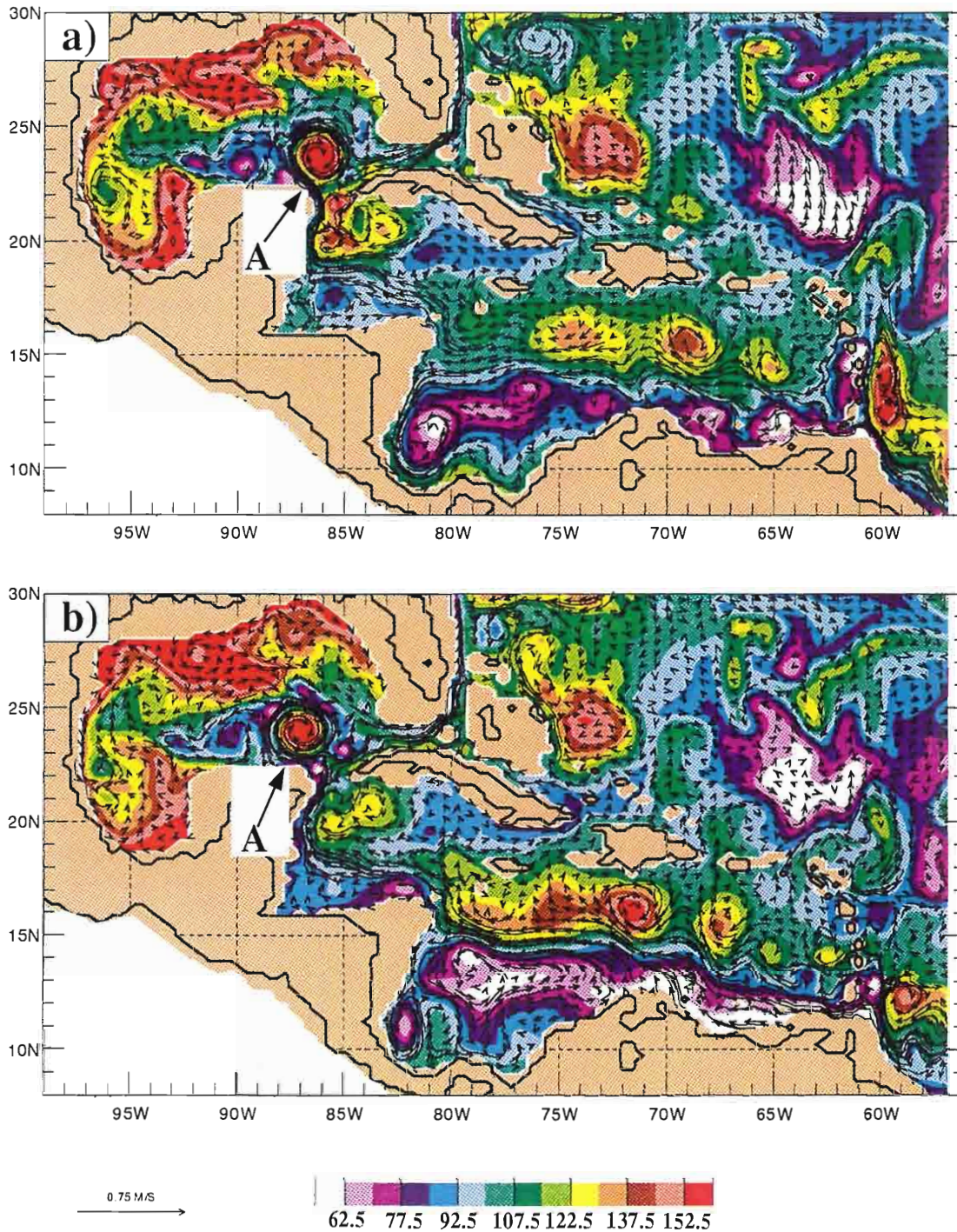
Figure 11. (a) **24** May 1987: Most of Eddy A is through the Yucatan channel and the Loop Current Eddy begins to separate. (b) **23** June 1987: Loop Current has separated.

Eddy "A". An analysis of potential vorticity for this year (1986) on either side of St. Vincent passage resulted in a cross correlation value of 0.54 at lag 90 days for simulation 1. This indicates that potential vorticity is not a constant through the passage, and at least some of the vorticity from the eastern side is advected to the west.

The eastern eddy was tracked in current fields from an initial position near 6° N and 49° W. This indicates that the eddy is most likely a Brazil retroflection eddy. Since a pioneering investigation into these eddies by Johns et al., [1990], retroflection eddies have been observed in Geosat data [Didden and Schott, 1993], drifter floats [Richardson et al, 1994], current meter arrays and numerical models [Fratantoni et al., 1995]. In all of these studies, approximately three retroflection eddies per year transited up the coast toward the Lesser Antilles. Unfortunately, drifter tracks through the Lesser Antilles are not reported, and may not have been calculated. Fratantoni [1995] reported that both the observed and modeled eddies decayed within 120 days of reaching the ridge between Tobago and Barbados (essentially the Lesser Antilles). It appears from the model simulation (Figure 6), that as the Brazil retroflection eddies decay, some of their vorticity can be advected into the Caribbean. One should be careful to note that the presence of Brazil retroflection potential vorticity does not, by itself, result in western eddy formation. The strength of the currents through the passages is also key which will be discussed shortly.

Several figures in the eddy track sequence demonstrate the flow of eddies from the Caribbean into the Loop Current system. In particular, Figure 10a, b has a well defined Loop Current eddy that is connected to an eddy on the Caribbean side of the Yucatan Channel. In figures 11a, b, the Figure 10a, b has a well defined Loop Current eddy that is connected to an eddy on the Caribbean side of the Yucatan Channel. In figures 11a, b, the

remnants of Eddy "A" have passed into the Loop Current eddy which has separated from the Loop. The connectivity of the Caribbean eddies to the Loop Current Eddy is qualitatively observable in this plot sequence, and will become quantitatively evident later on.

Cyclonic eddies in the eddy track sequence are observed to transit westward along an axis of 12° N until they are blocked by the Nicaraguan coast (see figures 8b and 11a), which then deflects the eddies southward along Panamanian and Columbian coasts.

The anticyclonic eddies transit in a fairly narrow corridor depicted in Figure 12. The corridor varies in width and is designed to encompass the ensemble of eddy tracks. The eddies were tracked using layer thickness maxima in the top layer. The layer thickness anomalies were averaged over the width of the corridor and in small increments of variable length. There are a total of thirty-two length increments. Each increment contains a time series of layer thickness (twelve years long). The long term mean (1981-1992) is subtracted.

The sum of layer thickness along this track reveals an annual and an intradecadal cycle of six years (Figure 13a). Although slight differences exist between simulations 1 and 2, the cycles are remarkably similar. There is an initial double negative peak at the beginning of 1982 and 1983. In simulation 1, the second peak is not as pronounced. These peaks are followed by a gradual build up of two years into the highest three positive peaks which occur in mid 1985, early 1986, and mid 1986. In simulation 1, the third peak is not as pronounced and there is a clearer definition between the second and third peaks. These peaks are followed by other positive peaks in early and late 1987. In the finite depth case these two peaks. These peaks are followed by other positive peaks in early and late 1987. In the finite depth case, these two

22

Fig. 12. Path representing average eddy track through the Caribbean.
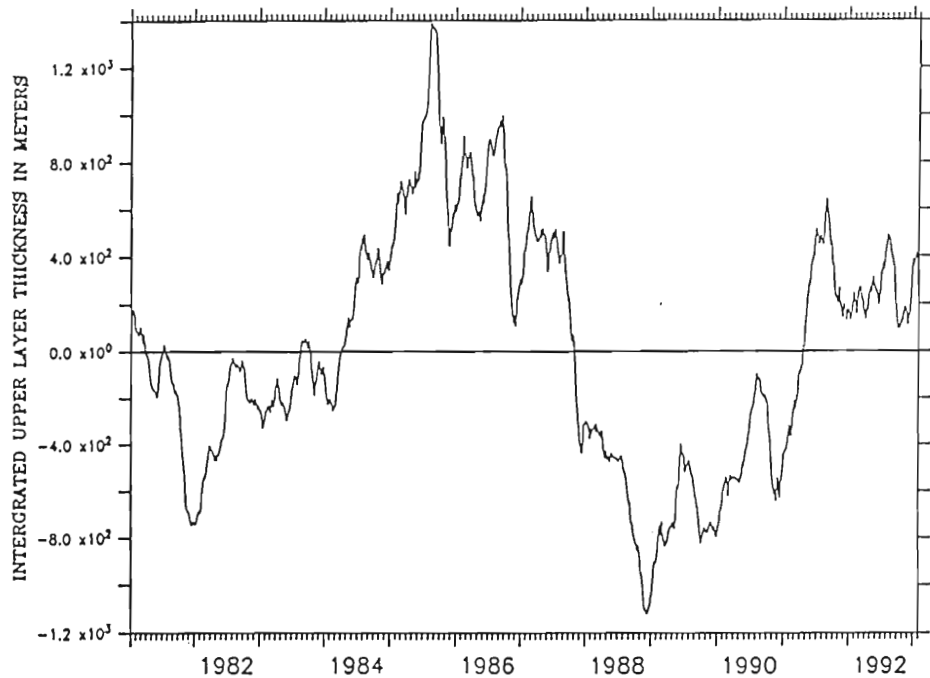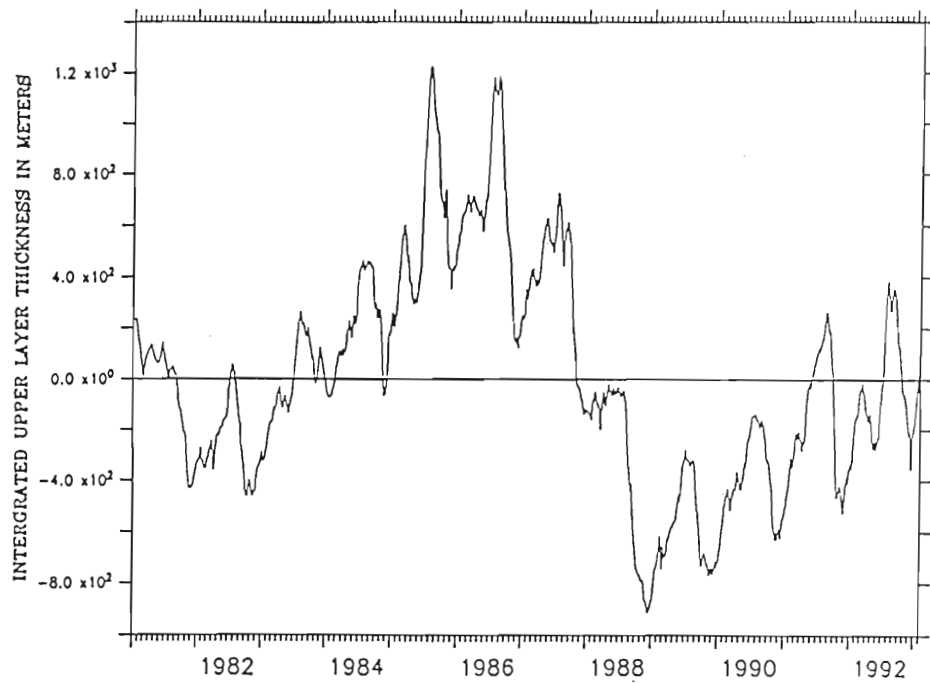
Fig. 13. (a) The sum of total layer thickness anomaly along the corridor in Figure 12 for the reduced gravity simulation. Total track distance is approximately 3800 km. Y-axis is sum of layer thickness in meters, and the x-axis is time. Data is available in 3.05 day increments from 1981 to 1994. The plot

Total track distance is approximately 3800 km. Y-axis is sum of layer thickness in meters, and the x-axis is time. Data is available in 3.05 day increments from 1981 to 1994. The plot shows an annual cycle and an intradecadal signal of several years. (b) same as above but for the finite depth simulation.

24

peaks appear as one broad peak. A rapid decrease over one year follows this final positive peak. There are three negative peaks in 1989, 1990, and 1991. In the remaining two years, the two simulations differ in amplitude but not phase. Both simulations exhibit peaks in late 1991 at the beginning of 1992. In simulation 2 (Figure 13b) the layer thickness is negative during this time, while in simulation 1 it is entirely positive.

Is the intradecadal cycle in the Caribbean remotely or locally generated? Since the connection between the Brazil retroflection eddies and the Caribbean eddies has already been demonstrated, a potential remote generation site could be the North Brazil Retroflection region. However, a kinetic energy analysis of this region indicates no intradecadal variability (Figure 14). The only regions in Figure 14 that possess the cycle are the Caribbean and the Gulf of Mexico. Although this suggests local generation for the intradecadal cycle, Hopfmüller diagram of currents outside of the region indicate otherwise.

Figure 15 is a Hopfmüller diagram of the u-component of velocity from a global linear simulation in which a strong Guyana current (see figure 2) is observed between 10 and 11° N along an axis of 58.2° W during the period of the intradecadal peak. Therefore, the intradecadal peak observed in the Caribbean eddies is also observed outside of the Caribbean.

The Guyana current continues northwestward to the Lesser Antilles where we see the pattern continued in the transport signal in the Lesser Antilles passages. Both the sum of the transports for all the passages in the Lesser Antilles (Figure 16b) and for the three southern most passages (Figure 16d) increase during the period of the intradecadal peak. The entire

25
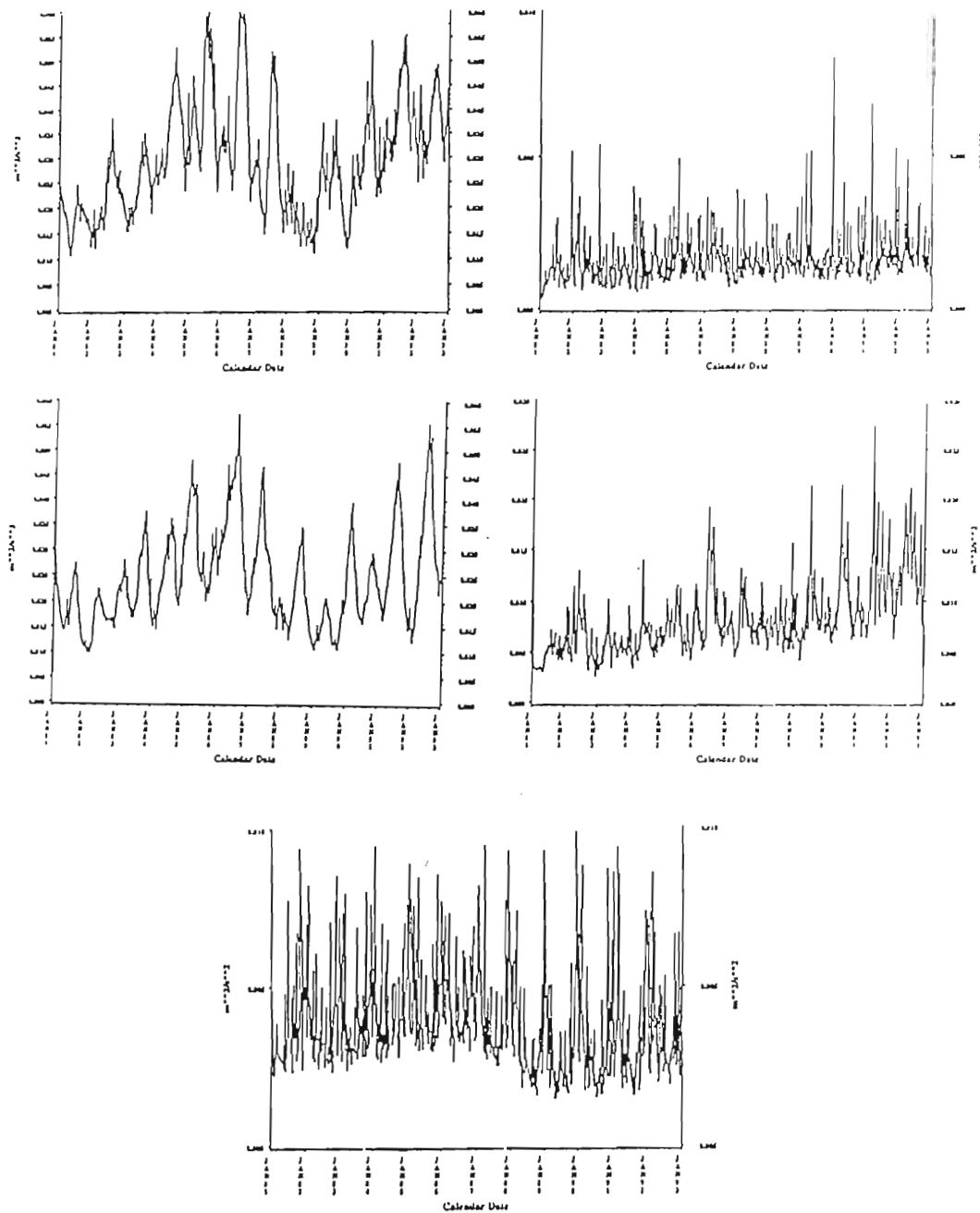
Fig. 14. Kinetic energy from the reduced gravity simulation spatially averaged over the following regions. (a) Caribbean: 9-18° N/ 64-85° W. (b) North Brazil Current: 2-14° N/ 44-60° W. (c) Gulf of Mexico: 23-28° N/ 88-95° W. (d) North Equatorial Current: 12-18° N/ 35-60° W. (e) Northeast of Caribbean: 18-31°N/ 50-74° W.

26
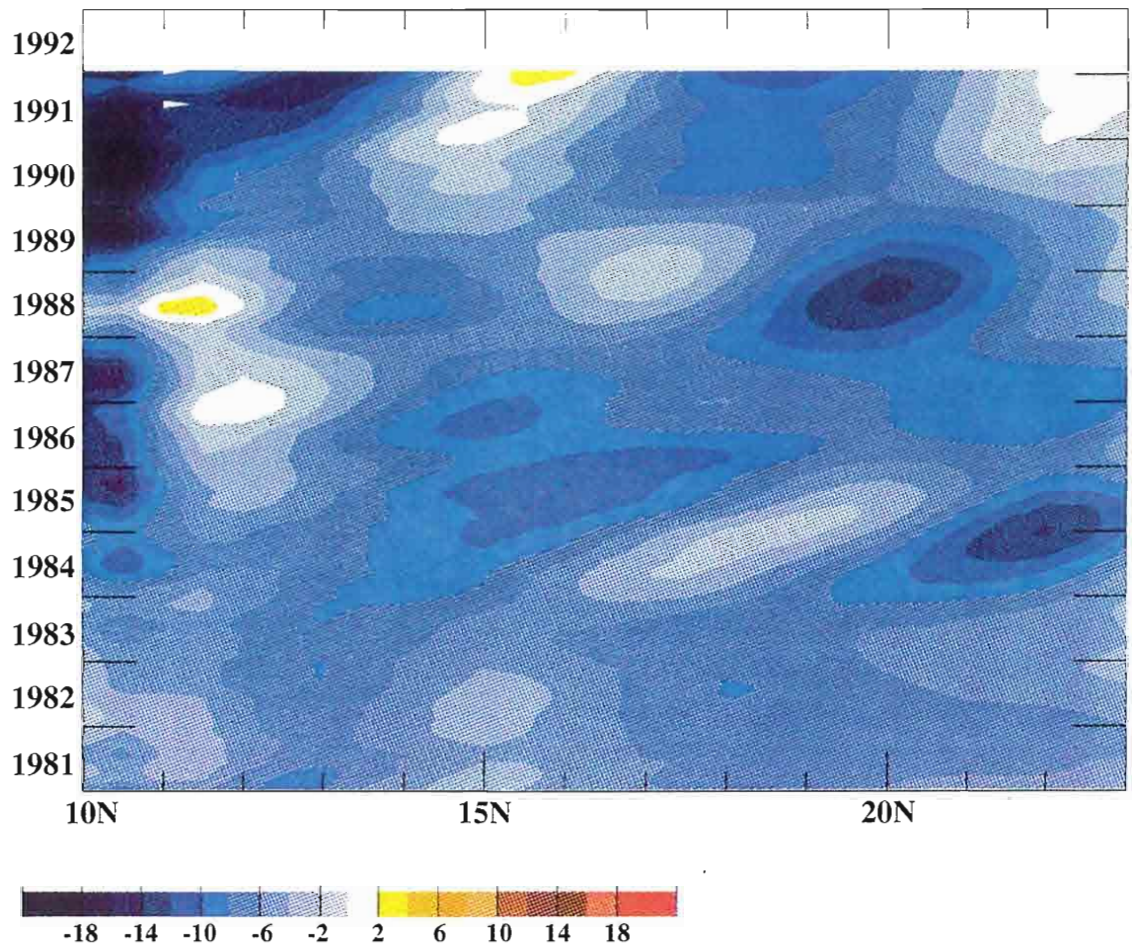
Figure 15. Phase plot of u-component of velocity from linear simulation along an axis of 58.2°W. Latitudes cover range from 10-23°N. Output has been smoothed by a one year running mean.
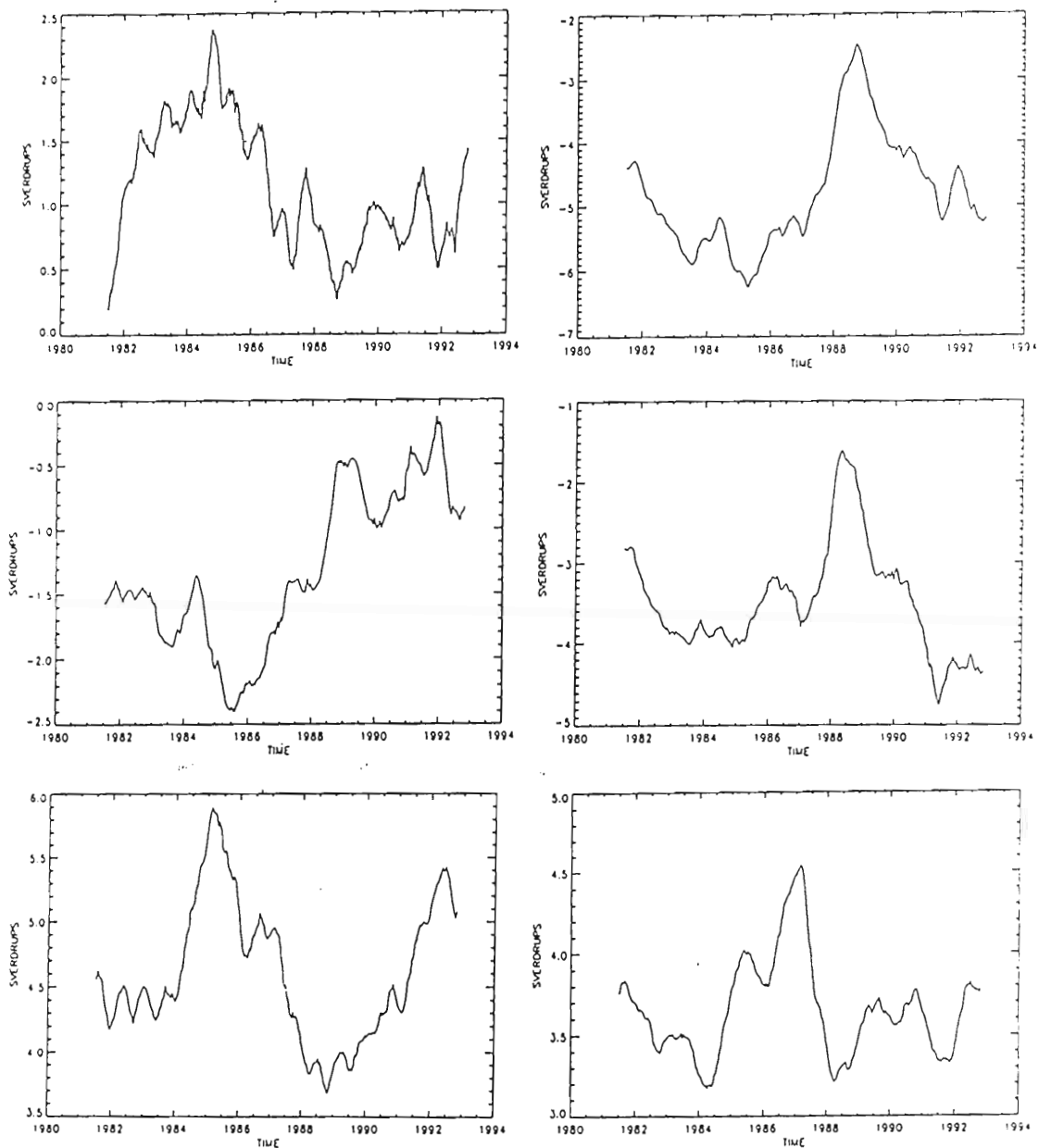
Fig. 16. Transport time series for various combinations of Caribbean passages from the reduced gravity simulation. Original data is available in daily increments. Each time series has been smoothed by a one year running mean. (a) Windward, Mona, Anegada. (b) All Lesser Antilles. (c) Guadeloupe, Dominique, and Martinique. (d) Grenada, St. Vincent, St. Lucia. (e) Yucatan Channel. (f) Florida Current at 27 degrees North (STACS).

pattern follows with a transport increase during periods when the Guyana Current is strong, and decreases with a decrease.

Eddies are formed west of the Lesser Antilles during these periods of increased flow through, which most likely indicates that the eddies are formed as a result of horizontal shear instability, a barotropic instability. Figure 17 indicates that considerable shear exists at the latitude of eddy formation. The initial eddy formation is weak, but the potential vorticity advected through St. Vincent passage is a finite amplitude perturbation on which horizontal shear instability can form. In Figure 18 the u-component of the internal Caribbean current is observed to be particularly intense during the period of the intradecadal peak. This intensity is most likely responsible for the intensification of the eddies in the interior of the basin. The dynamics involved in eddy formation then include an anomalously strong external current which increases transport through the Lesser Antilles and continues through the basin to the Yucatan Channel (see figure 16e for the Yucatan). Potential vorticity advected through the Lesser Antilles from decaying Brazil Retroflection eddies can act as a finite amplitude perturbation for horizontal shear instability. The eddies form west of the Lesser Antilles and intensify as they are advected across the basin in the Caribbean current.

Figure 19 is a map of the fraction of SSH varibility due to flow instabilities. Areas in the purple and blue are regions where the varibility is controlled largely by the wind forcing, whereas mesoscale flow instabilities are more important in the orange and red areas. Note that the majority of the Caribbean is controlled by wind forcing and is therefore

$$\frac{\partial \rho_k}{\partial t} + \vec{v}_k \cdot \nabla \rho_k =$$

$$\frac{\max(0, \omega_k)}{h_k}(\rho_{k+1} - \rho_k) + \frac{\max(0, -\omega_{k-1})}{h_k}(\rho_{k-1} - \rho_k) \qquad (2)$$

$$+ \frac{H_o}{h_k}\sigma_\rho(\hat{\rho}_k - \rho_k) - \delta_{1k}\frac{\gamma_t Q}{C_p \rho_o h_1} + \frac{K_H}{h_k}\nabla \cdot (h_k \nabla \rho_k)$$

$$\frac{\partial h_k}{\partial t} = \nabla \cdot \vec{V}_k = \omega_k - \omega_{k-1} \qquad (3)$$

See Appendix A for symbol definitions. A hydrodynamic version of this model is obtained by neglecting the density equation and retaining only the hydrodynamic part of the pressure gradient in the momentum equation:

$$\left(-h_k \sum_{l=1}^{n} G_{kl}\nabla(h_l - H_l)\right) \qquad (4)$$

A modified version of the 1/12° ETOPO5 bottom topography [NOAA, 1986] was used in the finite depth simulations that included realistic bottom topography. The topography data set was first interpolated to the model grid and then smoothed with a 9-point real smoother. This smoothing is to reduce the energy generation on small scales which are poorly resolved by the model. In the model integration, the amplitude of the topography above the maximum depth of 6500 m was multiplied by 0.78 to confine it to the lowest layer.

The model includes realistic coastline geometry, which has been extensively modified in the Caribbean region by Youtsey [1993]. This

geometry is determined by the 200 m depth contour of the topography which is the minimum depth in the model and represents the nominal shelf break. The model domain extends from 72° S to 71° N and has a horizontal resolution of 0.25° in latitude and 45/128° in longitude.

Seamounts and other rough bottom topography are confined to the bottom layer of the model. This removes the numerical difficulty that arises when moving interfaces intersect sloping topography [Hurlburt and Thompson, 1980]. Flow through straits with a shallow sill is constrained to small values below the sill depth.

Isopycnal outcropping and vertical mixing are permitted by entrainment from below when a specified minimum layer thickness, h_k^+, is reached. Mass is conserved within the layers, so that an accumulation of entrained mass in one layer is balanced by an equal amount of detrained mass elsewhere in the model domain, or via ports in the model boundary. For a description of the entrainment/detrainment scheme used see Shriver and Hurlburt, [1995]. The model boundary conditions are kinematic and no slip.

The thermal forcing in the thermodynamic version of the model is a relaxation of densities to climatological values [Levitus, 1982]. This density relaxation acts like an annual thermal forcing, which nudges the densities towards their climatological values.

Two versions of the model were used in this study: a thermodynamic 5.5 layer reduced gravity and a hydrodynamic six-layer finite depth with realistic bottom topography. The first simulation contains a representation of the first five baroclinic modes while the second represents these modes plus the barotropic mode. The thermodynamic experiment was spun up from rest at 0.5° for 259 years, and then at 0.25° for 36 years using the Hellerman-barotropic mode. The thermodynamic experiment was spun up from rest at 0.5° for 259 years, and then at 0.25° for 36 years using the Hellerman-

Rosenstein (HR) monthly winds. Similarly, the hydrodynamic experiment was spun up for 199 years at 0.5° and then for 29 years at 0.25°.

Both experiments were then forced with daily averaged European Center for Medium-range Weather Forecasts (ECMWF) hybrid winds. Hybrid refers to the replacement of the ECMWF mean with a Hellerman-Rosenstein climatological mean. This replacement was done for two reasons and is explained in detail in Metzger et al. [1992]. The global model simulations forced by pure ECMWF winds yielded a southern branch of the South Equatorial Current (SEC) and South Equatorial Counter Current (SECC) in the Pacific that were too strong compared with observations . Also, the simulated Pacific North Equatorial Current (NEC) was one to two degrees further north than its observed mean position. Simulations forced by Hellerman-Rosenstein winds did not exhibit this problem. With the hybrid winds, the annual mean is driven primarily by the HR winds, while the interannual variability is driven primarily by the ECMWF component.

The hybrid winds also make a smoother transition from the spin up, which uses HR winds, to the simulations with interannual forcing used here. The hybrid winds retain continuity in the mean field throughout the model run.

Model output used for this study includes velocity components (u, v) and layer thickness anomaly (h). Anomaly refers to the deviation from the initial layer thicknesses. Initial thicknesses for the 5.5 layers of the reduced gravity simulation are 80, 160, 160, 250, 350 meters, and infinitely deep. Similarly, the initial layer thicknesses for the six layers of the finite depth simulation are 155, 185, 210, 225, 225, and a thickness that varies with bottom depth. The subdomains of the global model domain used for this study are (8.0°-31.0° N / 61°-100° W) for the reduced gravity simulation (simulation 1), and (0.0°-

31.0° N /45°-100° W) for the finite depth simulation (simulation 2). They comprise the Caribbean/Gulf of Mexico regions and part of the North Atlantic.

Model output is available at every grid point at 3.05-day intervals for 14 years (1981-1994). In addition, NRL calculates transport (V) for each layer in selected passages including those of the Caribbean. The transport is output at daily intervals.

RESULTS

Mesoscale features in the Caribbean are observed in both model simulations. Anticyclonic eddies are observed to transit from the Lesser Antilles along an axis of 14-16° N until they are deflected northward by the Nicaraguan coast. Here the eddies often merge and intensify until they pass through the Yucatan channel (Figure 6).

Figures 6-11 are a case study of an anticyclonic eddy track through the Caribbean from simulation 1. This sequence is representative of an average track, with an eddy taking approximately ten months to transit the basin. The sequence occurs during the positive peak of the intradecadal variability (discussed in detail later). During the intradecadal peak, the anomalies are stronger, making the eddies easier to follow.

Throughout this sequence, Eddy "A" moves west/northwest and intensifies. Other anticyclonic eddies can be seen in various stages of transit. This is indicative of the complex and continuous flow of mesoscale variability that crosses the region. At present, no other study has demonstrated such an extensive eddy field for the Caribbean.

Several interesting events are highlighted by this eddy track sequence. In Figure 6a, a large anticyclonic eddy is observed on the eastern side of the Lesser Antilles. The arrows marking the currents indicate flow from the

eastern anticyclonic eddy through St. Vincent passage and into
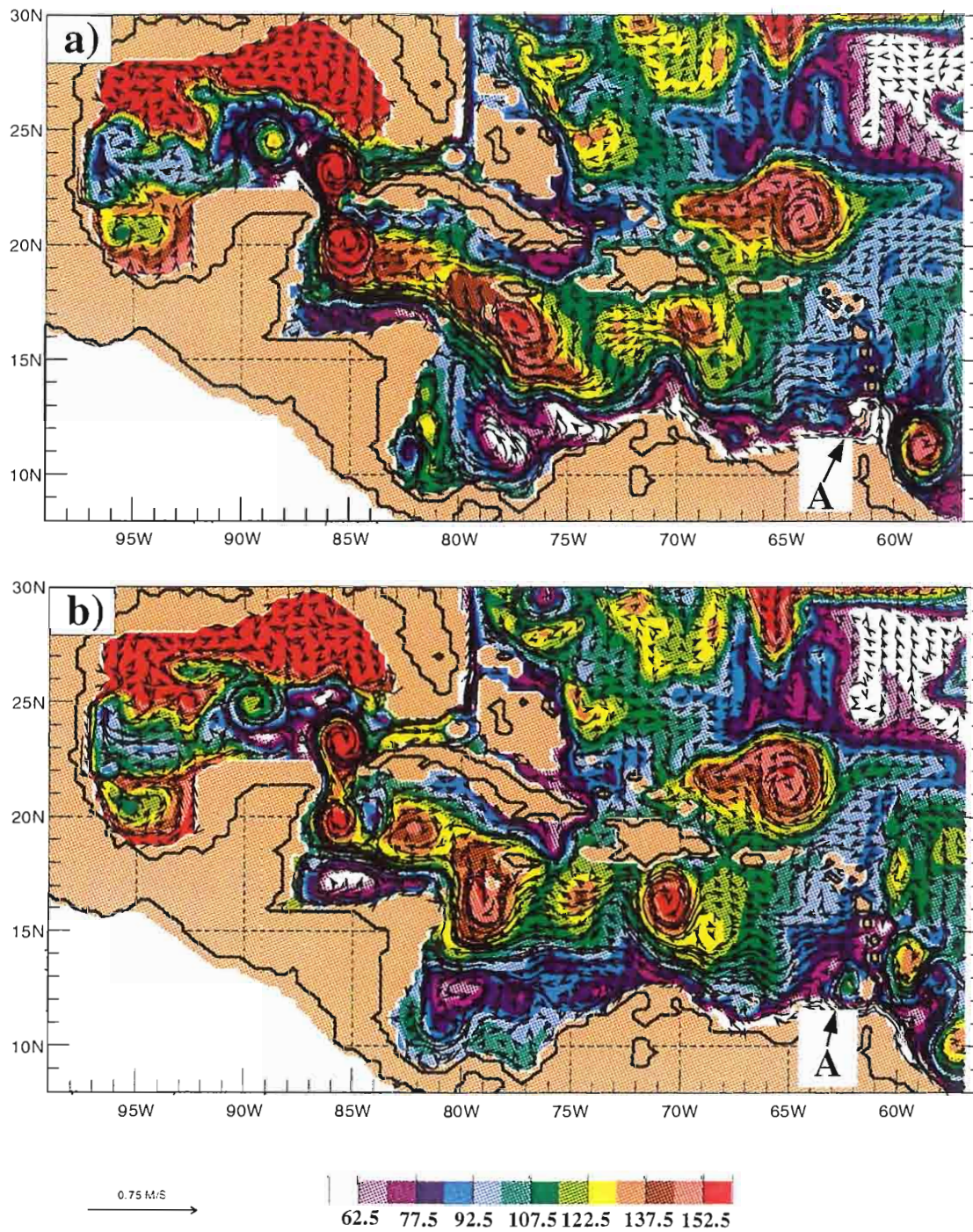
Figure 6. Upper layer thickness and velocity vectors from reduced gravity simulation. Eddy marked A will be tracked through subsequent plots. (a) 7 May 1986: Large anticyclonic eddy approaches the Lesser Antilles. (b) 7 June 1986: Eddy A has

Figure 6. Upper layer thickness and velocity vectors from reduced gravity simulation. Eddy marked A will be tracked through subsequent plots. (a) 7 May 1986: Large anticyclonic eddy approaches the Lesser Antilles. (b) 7 June 1986: Eddy A has intensified slightly.
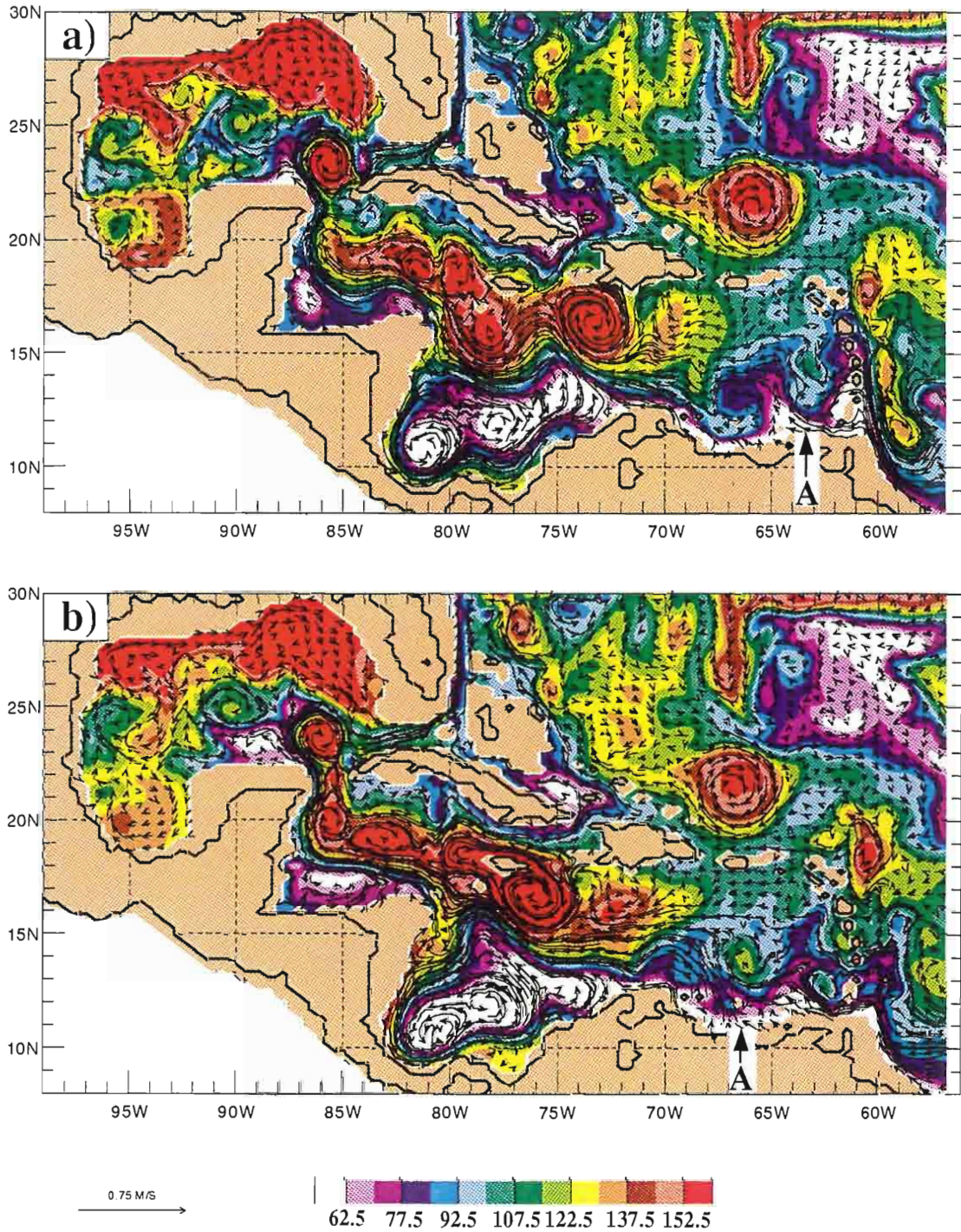
15

Figure 7. (a) 7 July 1986: Eddy A has transited to 63° W. (b) 7 Aug 1986: Eddy A has transited to 66° W and intensified further.

Figure 7. (a) 7 July 1986: Eddy A has transited to 63° W. (b) 7 Aug 1986: Eddy A has transited to 66° W and intensified further.
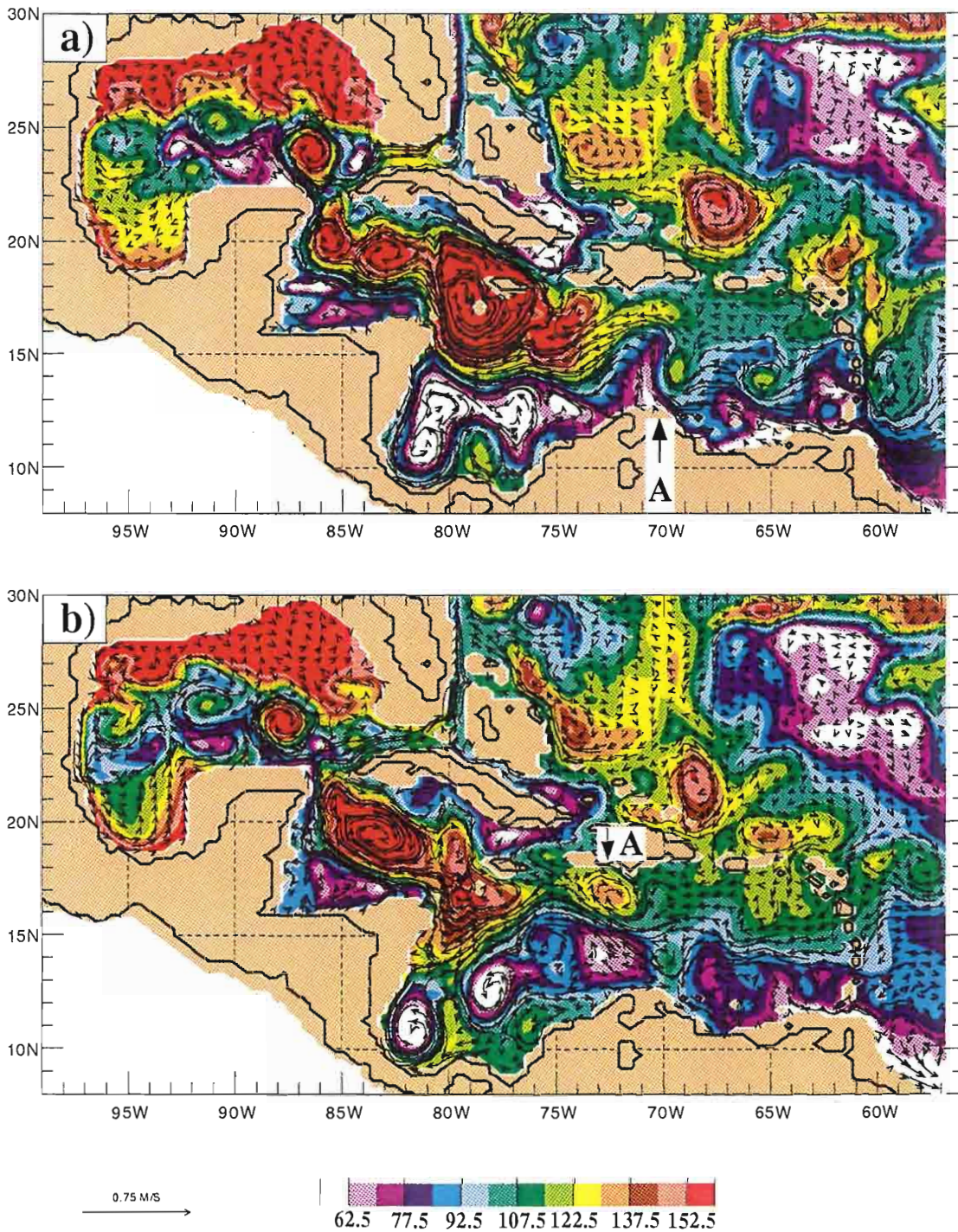
Figure 8. (a) 7 Sept 1986: Eddy A near 70° W. (b) 22 Oct 1986: Eddy A moves northwestward to 72° W.
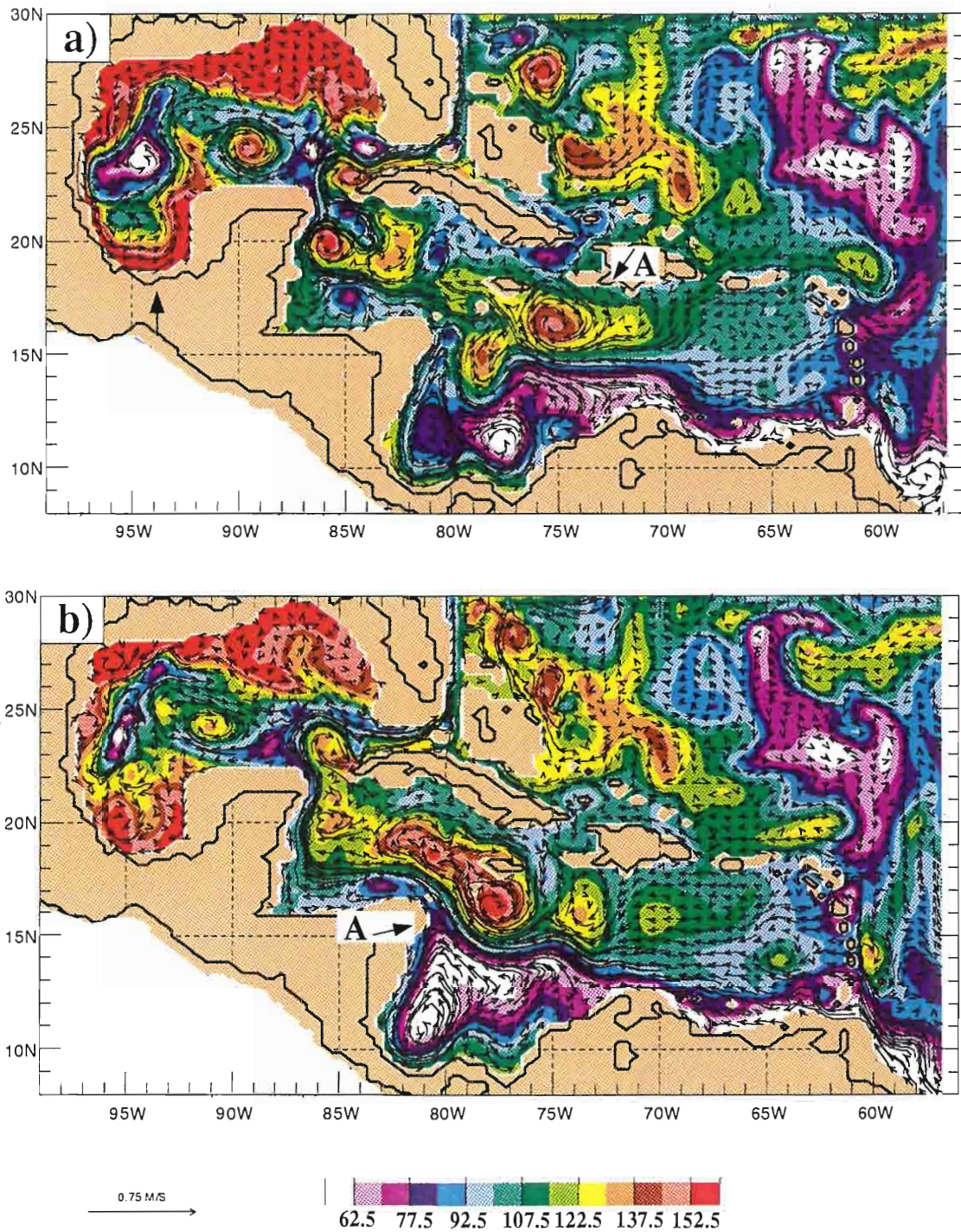
17

Figure 9. (a) 22 Dec 1986: Eddy A is along an axis of 15°N and continuing to intensify. (b) 6 Feb 1987: Eddy A is south of Jamiaca.

Figure 9. (a) 22 Dec 1986: Eddy A is along an axis of 15°N and continuing to intensify. (b) 6 Feb 1987: Eddy A is south of Jamiaca.

18
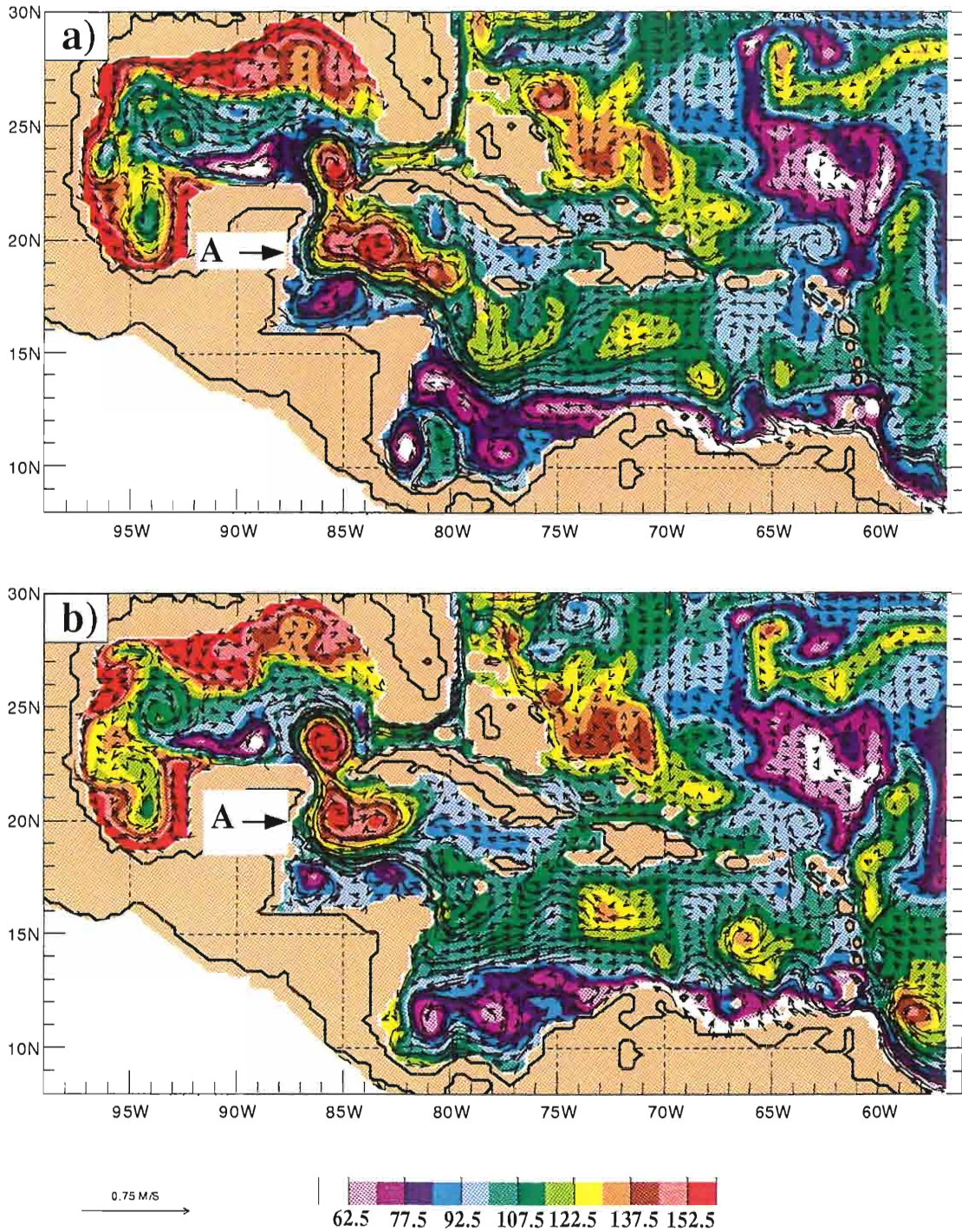
Figure 10. (a) 24 Mar 1987: Eddy A is approaching the Yucatan Channel. Previous eddy is connected to the Loop Current Eddy. (b) 23 April 1987: Material from Eddy A passess through the Yuctan Channel into the Loop Current.

undergo significant intensification. This intensification is due primarily to shear within the Caribbean current, which varies greatly over the intradecadal cycle. There is a significant correlation of 0.45 between the Loop Current Eddy Shedding and the eddies near the Lesser Antilles with a time lag of 11 months. In the reduced gravity simulation, 56% of the Caribbean eddies can be linked to Loop Current Eddy separation.

1

INTRODUCTION

The connectivity of eddy variability in the Caribbean Sea, the Gulf of Mexico, and the Atlantic Ocean is investigated using three global numerical ocean simulations. The model domain for all three simulations extends from 72° S to 71° N. Two simulations have a horizontal grid resolution of 0.25° in latitude and 45/128° in longitude. The third simulation has a horizontal grid resolution of 0.50° in latitude and 45/64° in longitude.

The first two versions of the model are a thermodynamic 5.5 layer reduced gravity and a hydrodynamic six-layer finite depth with realistic bottom topography. Both simulations were forced by daily ECMWF winds 1981-1994 and include realistic Caribbean geography. This geography plays a significant role in basin dynamics and will be discussed in the paper. The third simulation is a linear solution with the ECMWF hybrid wind forcing being scaled down by a factor of 1000. This scaling reduces the non-linear terms to negligible levels.

One advantage of layered ocean models lies in their modularity, which can be used to include or exclude dynamical processes. For example, the 5.5 layer reduced gravity simulation partially excludes baroclinic instability but allows for barotropic instability. This approach will be used to investigate the types of instabilities involved in eddy formation. Another example is the allows for barotropic instability. This approach will be used to investigate the types of instabilities involved in eddy formation. Another example is the linear simulation. In this simulation, the circulation revealed, can be

attributed to wind forcing only. This will be useful in determining the cause of Caribbean eddy formation. Section 2 presents the model design and gives more details on the forcing of each simulation. The connectivity of eddy variability in the Caribbean, Gulf of Mexico, and the Atlantic Ocean is discussed in Section 3. Topics include (1) the influence of the Atlantic Ocean on the formation of Caribbean eddies and its role relative to flow instabilities within the Caribbean, (2) a description of the eddies, their mean pathways, velocities, and annual and intradecadal cycles of eddy activity, (3) an investigation into the origins of the intradecadal cycle including a kinetic energy analysis of several regions external to the Caribbean, (4) a discussion of the local wind stress and its effect on eddy formation and the intradecadal cycle, (5) the relationship between Caribbean eddies and the eddy shedding of the Loop Current in the Gulf of Mexico, (6) a model data comparison between Geosat Caribbean eddies and model eddies and, (7) a discussion of transport connectivity within the Florida Current system. Section 4 contains the summary and conclusions.

The Caribbean is a semi-enclosed sea bounded on the west and north by a chain of closely spaced islands that act as a sieve for inflow from the Atlantic Ocean (Figure 1). A great deal of uncertainty exists about the distribution of inflow through the various Caribbean passages. However, the general circulation within the basin has been studied since the early 1960's. Observations show that the Caribbean circulation is characterized by a northwestward flowing current that bisects the basin and exits through the Yucatan Channel (Figure 2). Other features include a semi-permanent cyclonic circulation in the Columbian basin, here depicted in the mean currents from the reduced gravity simulation (Figure 3). In the numerical cyclonic circulation in the Columbian basin, here depicted in the mean currents from the reduced gravity simulation (Figure 3). In the numerical
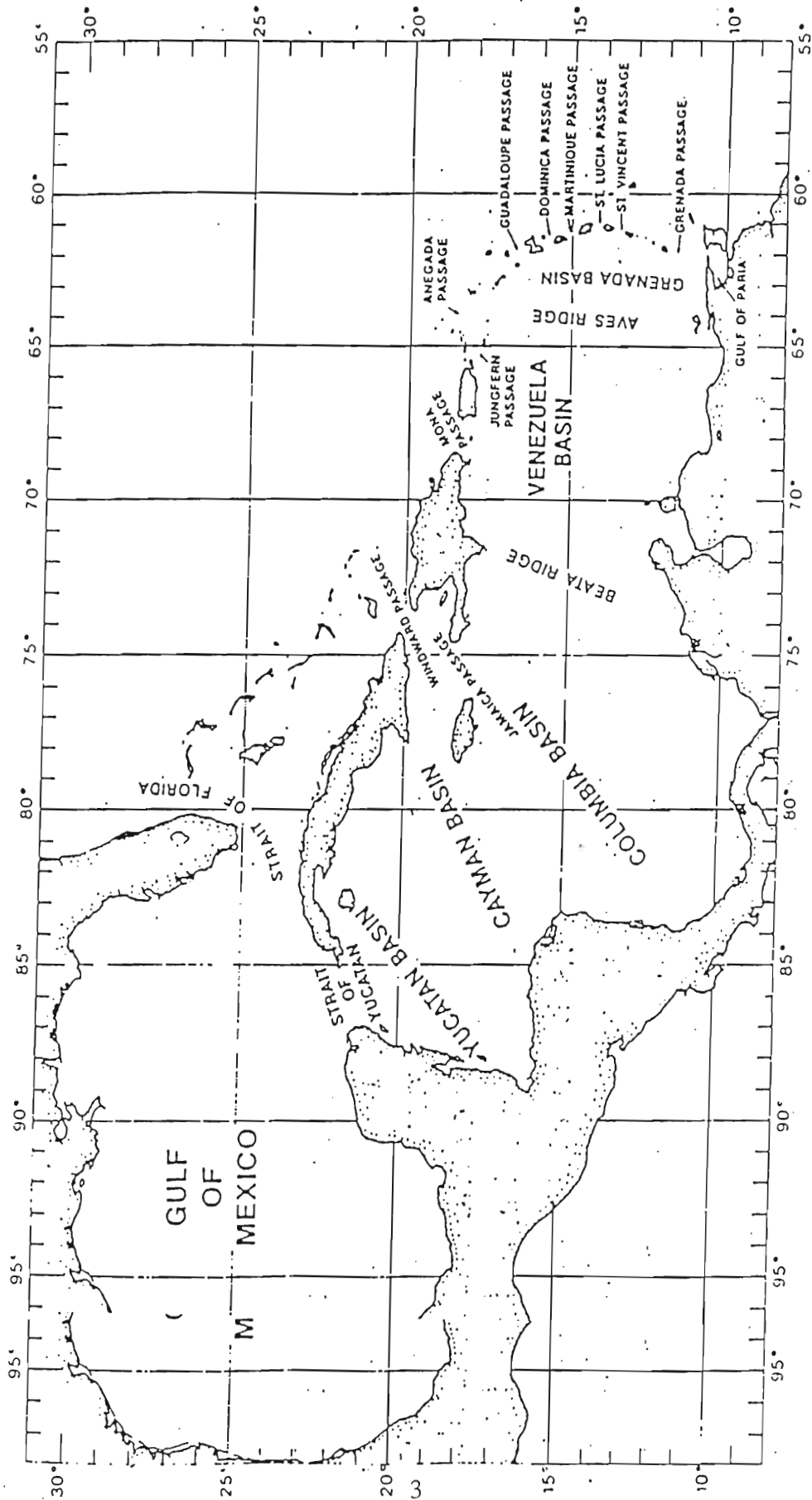
Fig. 1. Caribbean geography and place names [from Kinder et al., 1985]
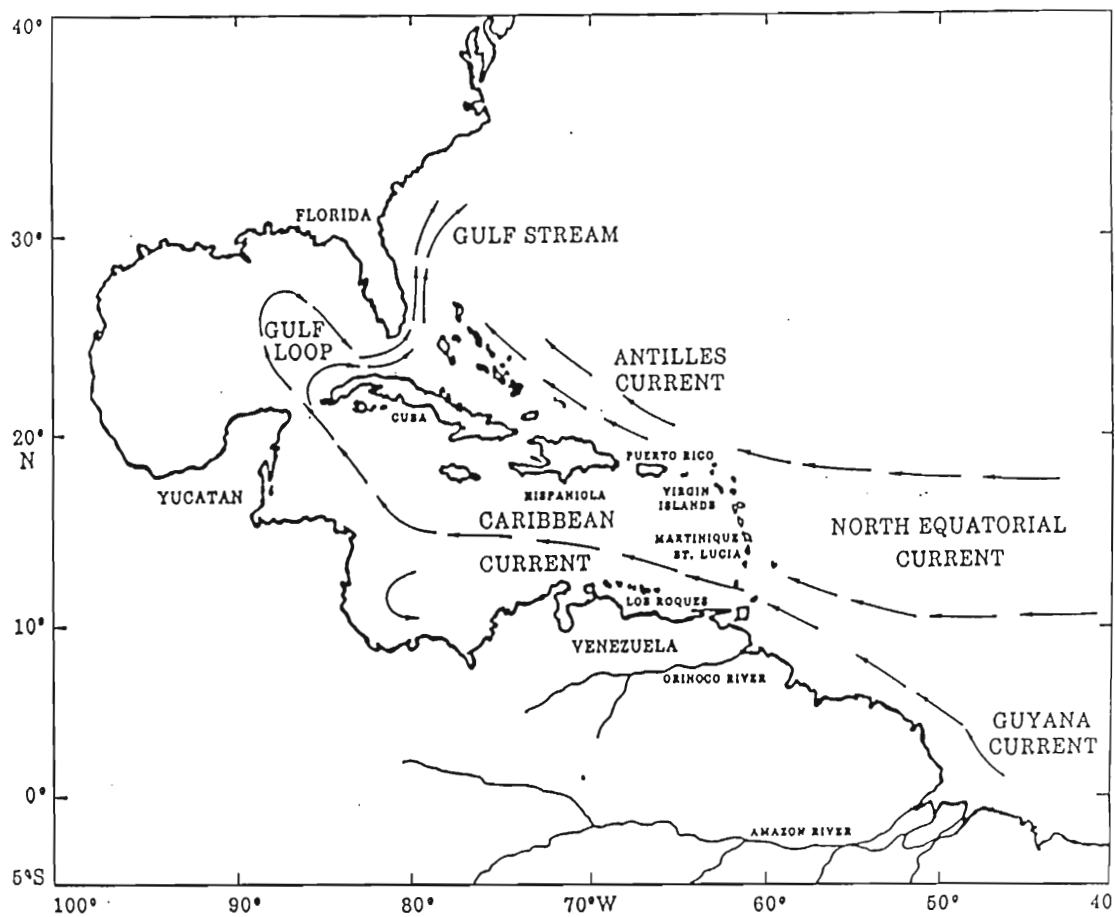
Fig. 2. Generalized Caribbean circulation drawn from
Pilot Charts [From Duncan, et al., 1982]
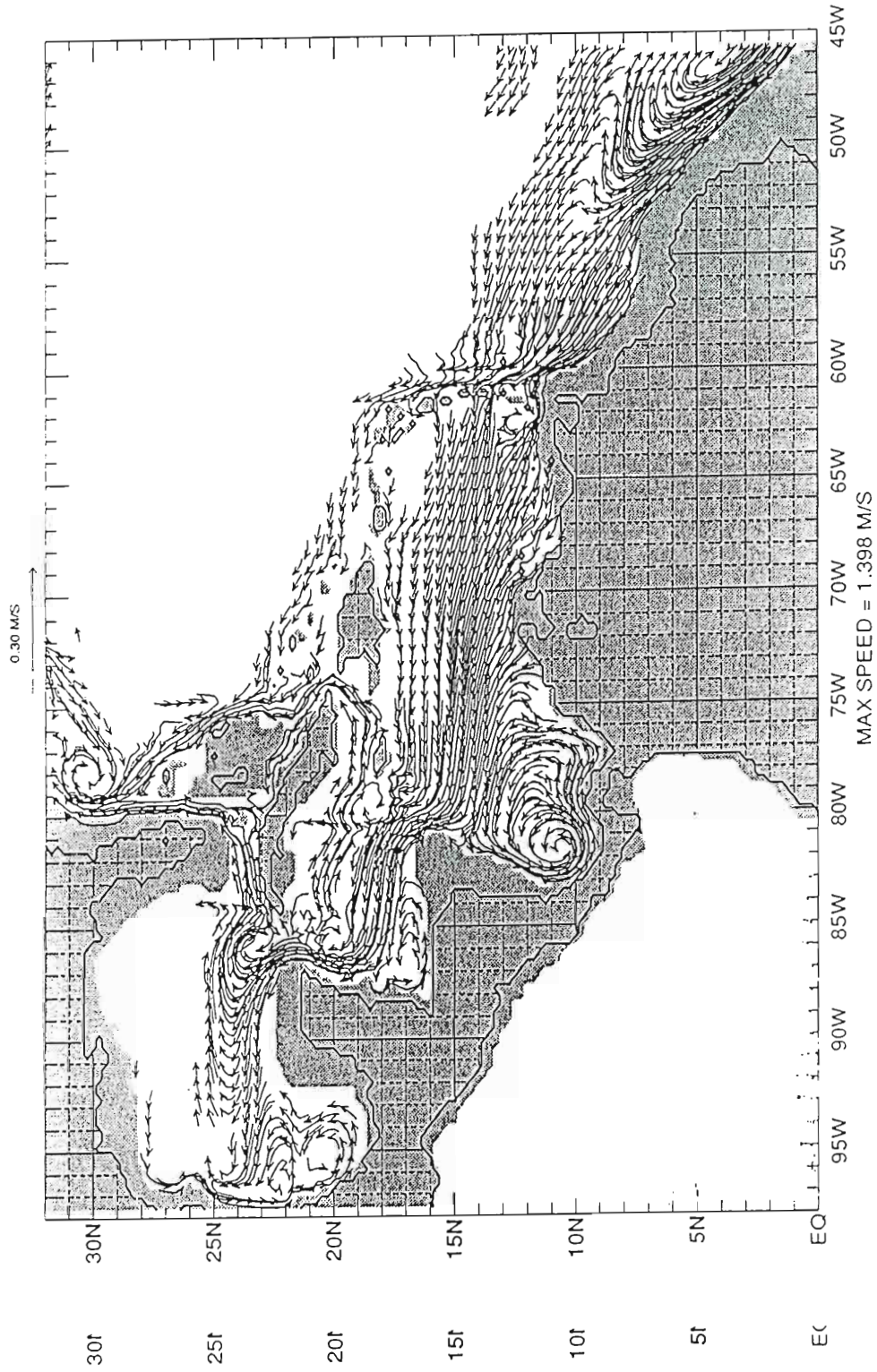
Fig. 3. Mean annual currents 1981-1991 for layer one of the reduced gravity simulation.

5

simulations, the Lesser Antilles acts as a barrier in space to eddy kinetic energy except through the three southern most passages (Figure 4). The energy from this region then transects the Caribbean basin along the axis of the Caribbean current. Many aspects of Caribbean circulation, including mesoscale variability, are summarized by Kinder et al., [1985]. Maul [1993] also presents an overview including the environmental and socio-economic implications of global climate change in the Caribbean.

Caribbean eddies have been discussed in the literature [Fu and Holt, 1983; Heburn et al., 1982, Ingham and Mahnken, 1966; Kinder, 1983; Lemming, 1971; Molinari et al., 1981; and Nystuen and Andrade, 1993], but these studies have been limited in spatial and temporal resolution. The utilization of a global numerical model allows for research at time and space scales currently unfeasible observationally.

Pertinent to this study is the Loop Current in the Gulf of Mexico region. The Loop Current enters the Gulf of Mexico through the Yucatan Channel and traces an anticyclonic path that varies in northward penetration, before turning southward and exiting through the Florida Strait (Figure 5). The Loop Current bends westward and sheds large anticyclonic eddies that range in diameter from 300 to 400 km [Vukovich et al., 1979]. The periodicity and cause of this eddy shedding will be reviewed in Section 3 coincident with a discussion of how Caribbean eddies affect both aspects of the Loop Current in the Gulf of Mexico.
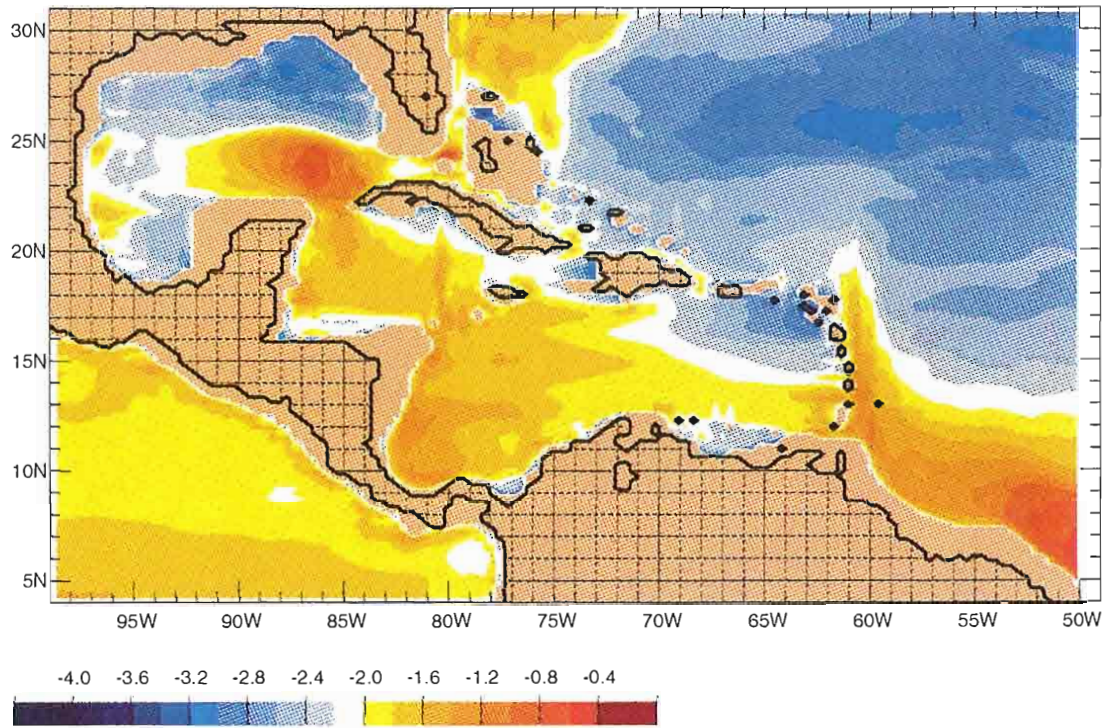
Figure 4. Contours for the log of mean eddy kinetic energy in m^2s^{-2} for layer one of the reduced gravity simulation.
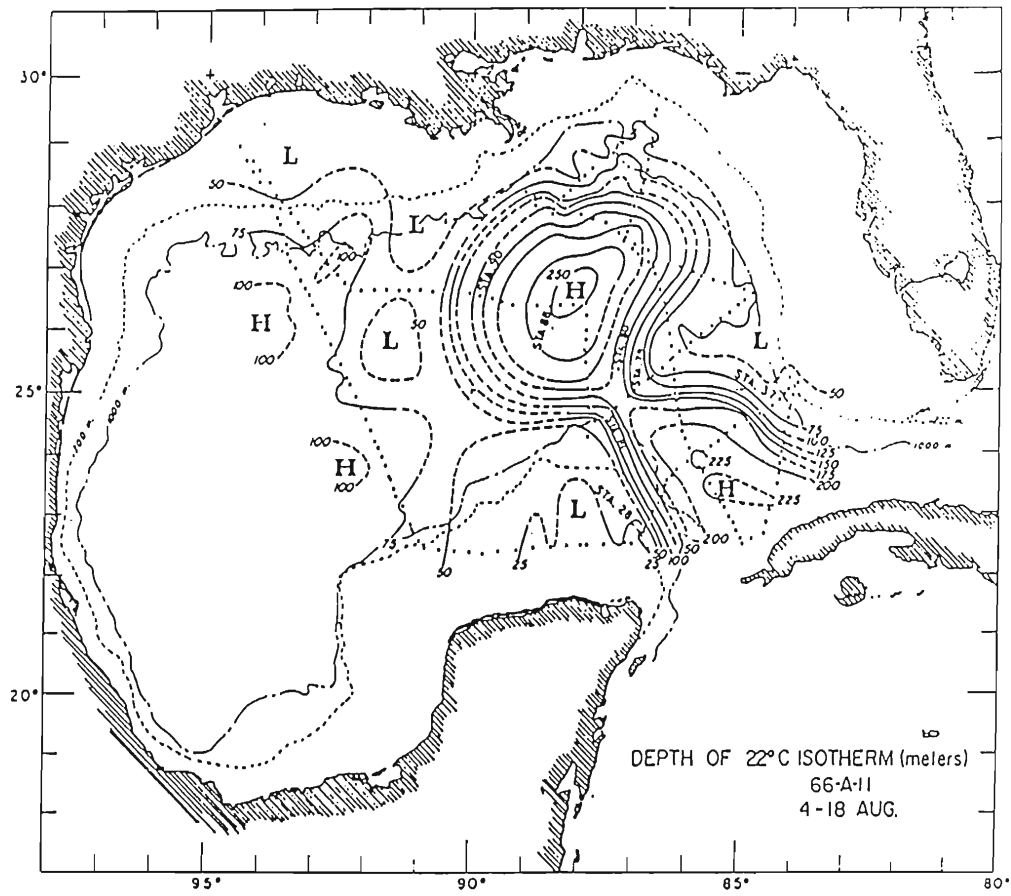
Fig. 5. Topography of the 22°C isothermal surface, 4-18 August 1966 (Alaminos cruise 66-A-11) [from Leipper, 1970]

8
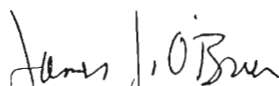
MODEL AND EXPERIMENTS

The model used in this study is the Naval Research Laboratory 's (NRL) global multi-layer model [Wallcraft, 1991], which is based on the semi-implicit, free surface model of Hurlburt and Thompson [1980]. The model is formulated using an Arakawa 'C' grid [Mesinger and Arakawa, 1976] with an explicit numerical scheme for the reduced gravity simulations and a semi-implicit scheme for the finite depth simulations.
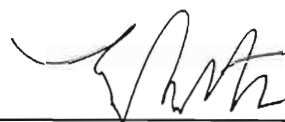
The equations for the n-layer finite depth, thermodynamic model are, for layers k=1,...,n:

$$
\frac{\partial \vec{V}_k}{\partial t} + (\nabla \cdot \vec{V}_k + \vec{V}_k \cdot \nabla) \vec{V}_k + \hat{k} \times f \vec{V}_k =
$$

$$
\max(0, -\omega_{k-1}) \vec{v}_{k-1} + \max(0, \omega_k) \vec{V}_{k+1} - (\max(0, -\omega_k)
$$

$$
+ \max(0, -\omega_{k-1})) \vec{v}_k + \max(0, C_M \omega_{k-1})(\vec{v}_{k-1} - \vec{v}_k) +
$$

$$
\max(0, C_M \omega_k)(_{k+1} - \vec{v}_k) - h_k \left(\sum_{l=1}^{n} (G_{kl} \nabla(h_l - H_l) + h_l \nabla G_{kl}) \right) \tag{1}
$$

$$
- \frac{g}{\rho_0} \left(\sum_{l=1}^{k-1} h_l + \frac{h_k}{2} \right) \nabla \rho_k) + (\vec{\tau}_{k-1} - \vec{\tau}_k) / \rho_o + A_H \nabla^2 \vec{V}_k
$$

The members of the Committee approve the thesis of Sylvia Murphy defended on 11 October 1995.

James J. O'Brien
Professor Directing Thesis

Lita M. Proctor
Committee Member

Harley E. Hurlburt
Committee Member

Wilton Sturges
Committee Member

Table of Contents

iii

List of Figures

List of symbols

$\vec{v}_k$ = k-th layer velocity

h_k = k-th layer thickness

$V_k = h_k \vec{v}_k$

H_k = k-th layer thickness at rest

$$H_n = D(x,y) - \sum_{l=1}^{n-1} H_l$$

$D(x,y)$ = total ocean depth at rest

ρ_k = k-th layer density, constant in space and time

$$G_{kl} = \begin{cases} g & \\ g - g(\rho_1 - \rho_k)/\rho_o & \end{cases} \quad \text{for} \quad \begin{array}{l} 1 \le k \\ 1 > k \end{array}$$

f = Coriolis parameter

A_H = coefficient of horizontal eddy viscosity

C_b = coefficient of bottom friction

C_k = coefficient of interfacial friction

$\vec{c}_k$ = coefficient of interfacial friction

$\vec{\tau}_w$ = wind stress:

$$\vec{\tau}_k = \begin{cases} |\vec{\tau}_w| & k = 0 \\ C_k \rho_o |\vec{v}_k - \vec{v}_{k+1}| (\vec{v}_k - \vec{v}_{k+1}) & \text{for} \quad k = 1...n-1 \\ C_b \rho_o |\vec{v}_n| \vec{v}_n & k = n; \end{cases}$$

$$\omega_k = \begin{cases} 0 & k = 0, n \\ \max(0, \omega_k^+) - \max(0, \omega_k^-) - h_k \hat{\omega}_k & \text{for} \quad k = 1...n-1 \end{cases}$$

$$\omega_k^+ = \tilde{\omega}_k (\max(0, h_k^+ - h_k)/h_k^+)^2$$

$$\omega_k^- = \tilde{\omega}_k (\max(0, h_k - h_k^-)/h_k^+)^2$$

$$\hat{\omega}_k = \frac{\iint (\omega_k^+ - \omega_k^-)}{\iint \Omega_k}$$

$\hat{\omega}_k = $ k-th interface reference vertical mixing velocity

$h_k^+ = $ k-th layer thickness at which entrainment starts

$h_k^- = $ k-th layer thickness at which detrainment starts

$\Omega_k(x, y) = $ k-th interface global mixing correction factor

$C_M = $ coefficient of additional interfacial friction associated with entrainment

$K_H = $ coefficient of horizontal density diffusivity

$\sigma_{\rho_H} = $ reference coefficient of density climatology relaxation

$\sigma_\rho = $ reference coefficient of density climatology relaxation

$\hat{\rho}_k(x, y) =$ k-th layer density climatology

$H_o =$ constant reference layer thickness

$Q =$ surface heat flux

ABSTRACT

A set of numerical simulations is used to investigate the connectivity of mesoscale variability in the Atlantic Ocean, the Caribbean, and the Gulf of Mexico. The primitive equation models used for these simulations have a free surface and realistic coastline geometry including a detailed representation of the Lesser Antilles island arc. Two simulations have $1/4°$ resolution and include a 5.5-layer reduced gravity and a 6-layer with realistic bottom topography. The third simulation is a $1/2°$ linear model.

In the two non-linear numerical simulations, potential vorticity from decaying Brazil Retroflection eddies can be advected through the Lesser Antilles. This potential vorticity acts as a finite amplitude perturbation for horizontal shear instability and mesoscale features form as a result. The strength of the current through the Lesser Antilles is key to this formation. Transport increases through the passages when the strength of the Guyana Current is anomolously strong which indicates that the pattern is observed externally as well as internally to the Caribbean. The pattern occurs on an intradecadal cycle of six years and is observed in the currents of the linear simulation as well transports and Caribbean eddies of the non-linear simulation. The eddies are primarily anticyclonic and transits a narrow corridor across the Caribbean basin along an axis of 14° to 15° N with an average speed of 0.15 m/s. It takes them an average ten months to transit from the Lesser Antilles to the Yucatan Channel. Along the way, the eddies average speed of 0.15 m/s. It takes them an average ten months to transit from the Lesser Antilles to the Yucatan Channel. Along the way, the eddies